

Supplementary Information

Flexible Covalent Organic Framework Membranes with Linear Aliphatic amines for Enhanced Organic Solvent Nanofiltration

Biswajit Mishra and Bijay P Tripathi*

Functional Materials & Membranes Laboratory, Department of Materials Science and Engineering, Indian Institute of Technology Delhi, Hauz Khas, New Delhi, 110016, India.

Corresponding Author Email: bpatripathi@mse.iitd.ac.in; drbpatripathi@gmail.com

Table of contents

Section		Page no.
S1	Materials, methodologies, and instrumentation	S2
S2	Solid state ¹³ C NMR of TFG-EDA, TFG-DETA, and TFG-TETA	S12
S3	Morphological analysis	S13
S4	FTIR of COF membranes	S14
S5	X-ray photoelectron spectroscopy analysis	S15
S6	BET summary	S16
S7	TGA analysis	S13
S8	PXRD of COF membranes	S17
S9	Static BSA adsorption test	S20
S10	Additional information about Atomic force microscopy	S21
S10	Molecular weight cut-off analysis	S22
S11	Additional information for OSN performance	S23
S12	Dynamic antifouling performance	S30
S13	Structural Modelling and refinement of COFs	S31
S14	References	S41

S1. Materials, methodologies, and instrumentation

S1.1. Materials

Phloroglucinol, trifluoroacetic acid, and hexamethylene tetramine were purchased from TCI, Japan. 1,3,5-triphlorofluoroglucinol was prepared using previously reported literature, and the purity was confirmed using NMR (^1H and ^{13}C) and FTIR. Ethylene diamine (EDA), diethylene triamine (DETA), triethylene tetraamine (TETA), acetic acid, and all other solvents/chemicals were procured from Sigma-Aldrich (USA) and used as received. Methylene blue, Congo red, crystal violet, brilliant blue, and all solvents were purchased from CDH (P) Ltd. India. The polyethylene terephthalate (PET) track etched microporous membranes (pore size = 0.20 μm , pore density = 5×10^8 pores cm^{-2}) were acquired from it4ip, Belgium. Prior to interfacial polymerization, PET membranes were thoroughly washed with isopropanol/water to remove any impurities. For all experimental purposes, Millipore deionized water was used.

S1.2. Methodologies

S1.2.1. Synthesis of 1,3,5-triphlorofluoroglucinol (TFG)

TFG was synthesized according to a literature procedure with slight modifications.¹ Initially, 36 mmol of hexamethylenetetramine and 16.33 mmol of phloroglucinol were mixed in a two-necked round bottom flask under an N_2 environment. The mixture was purged with N_2 for 30 minutes, after which 33 mL of trifluoroacetic acid was slowly added dropwise while vigorously stirring. The resulting solution was then heated at 100°C for 2.5 h under an N_2 atmosphere. After that, 100 mL of 3M HCl was added to the reaction mixture and stirred for another hour at 100 °C. The solution was then cooled, filtered through celite, and extracted with dichloromethane. Anhydrous magnesium sulfate was added to the DCM solution and stirred overnight to remove trace amounts of water. Finally, the solution was filtered, and the resulting off-white product was obtained by rotary evaporation. The product was confirmed using NMR and FTIR and stored at 4 °C.

S1.2.2. Synthesis of COF thin film over porous support via interfacial polymerization

COF nanofilms were fabricated on a porous PET support membrane using an interfacial polymerization technique with a similar concentration of all monomers, catalysts, and solvents. The thickness of the COF layer was optimized by adjusting the interfacial polymerization time.

Prior to interfacial polymerization, the PET membrane was treated with 1 wt% PVA to improve the interaction of the COF layer with the support membrane. The PET membranes were placed on a custom-made stainless-steel plate using double-sided adhesive tape (**Figure S2**). The COF thin film was prepared in a 250 mL beaker at room temperature. Briefly, 0.045 mmol of Scandium triflate was added into 50 mL of an aqueous phase (**Solution A**) and poured onto the support membrane. In another beaker, 0.3 mmol of TFG was mixed in 47.5 mL of xylene and 2.5 mL of DCM and stirred gently to obtain a clear solution (**Solution B**). Then, 0.45 mmol of diamine was added to solution B and stirred for 120 sec, resulting in a turbid yellowish solution. Solution B was then slowly poured into the aqueous phase using a funnel without disturbing the mixture. The beaker was covered with a glass plate to avoid airflow and kept undisturbed during polymerization. After different intervals of polymerization time, the stainless-steel plate was lifted upward to transfer the COF film to the porous PET support. The fabricated COF membrane was thoroughly washed with DMAC, water, and ethanol, followed by ambient drying at 35 °C and vacuum drying at 45 °C. The resulting membrane over support was denoted as TFG-EDA. Similarly, TFG-DETA and TFG-TETA were prepared using a similar approach but with different diamines, such as DETA and TETA. To obtain a self-standing COF film, interfacial polymerization was conducted for 72 h, followed by washing with DMAC, water, and ethanol and vacuum drying at 35 °C for 24 h.

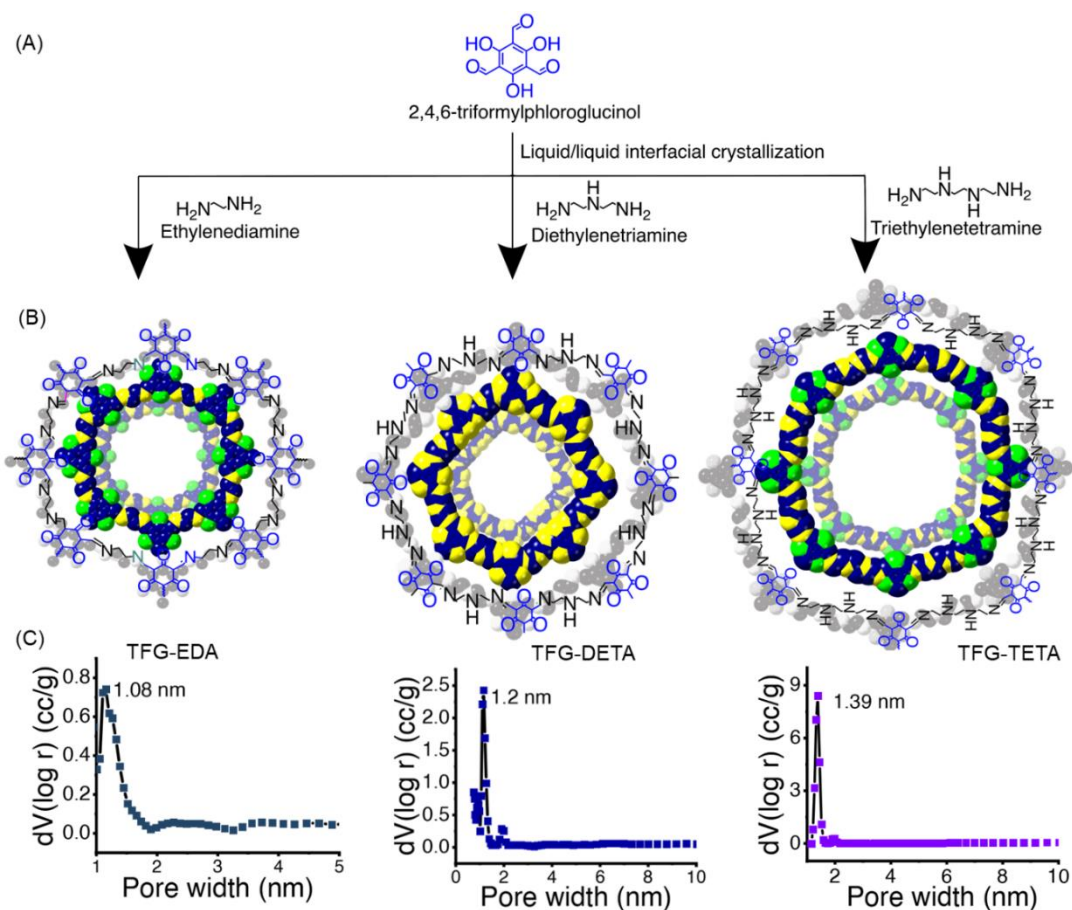


Figure S1| Schematic representation of COFs using different diamine monomers (A), Chemdraw and modelled structures of all COFs (B), pore-size distribution of corresponding COF membranes (C).



Figure S2| Fabricated stainless-steel plate for transferring the COF nanofilm to the porous substrate after interfacial polymerization.

S1.2.2 (a) Control of COF film thickness

The thickness of the COF film can be controlled by varying several parameters, including monomer concentration, polymerization time, etc. Herein, we regulated the COF layer thickness by changing the interfacial polymerization time. The detailed synthesis conditions are discussed in the previous section. For instance, after adding the organic phase to an aqueous solution, instantly within 15 min of polymerization, an ultrathin film appeared at the interface. In the initial stages, the film was mechanically unstable. Therefore we allowed a longer polymerization time to achieve a defect-free large-area COF membrane over the polymeric membrane support. To assess the effect of polymerization time, the COF layer was transferred to the PET support at different time intervals, and FESEM cross-sectional analysis was performed to measure the film thickness. As observed in **Figure S3**, all the COF membrane exhibits ~55 nm of thickness with a polymerization time of 30 min. At 120 min of polymerization time, the thickness of TFG-EDA, TFG-DETA, and TFG-TETA was found to be 116 ± 4 , 120 ± 5 , and 115 ± 6 nm, respectively. The mean roughness of the TFG-EDA, TFG-DETA, and TFG-TETA layers is 42 ± 6 , 37 ± 3 , and 44 ± 4 nm, respectively. The results of our study indicate the control of COF thickness and roughness by tuning the polymerization time, which can be applied to similar kinds of COF film preparation for future research.

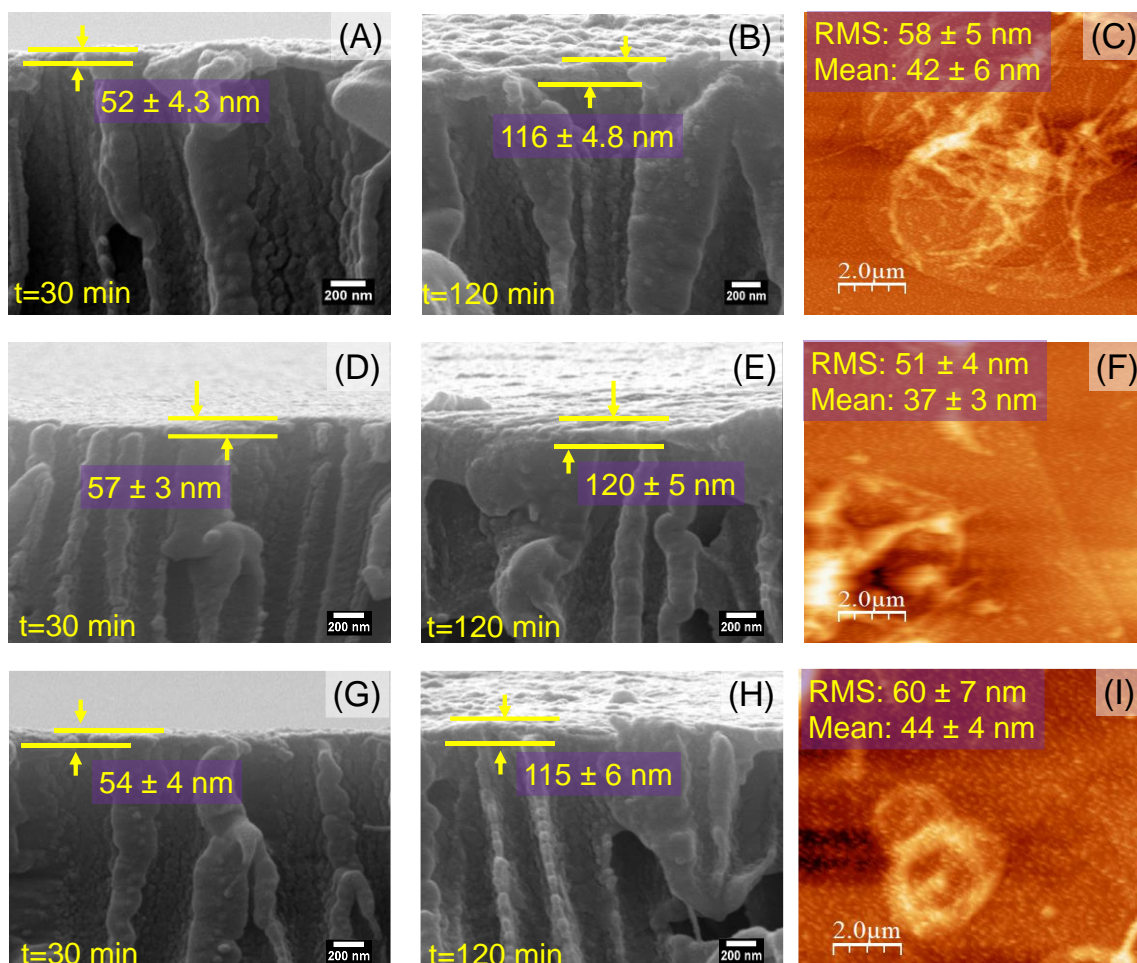


Figure S3| Effect of interfacial polymerization time on COF layer thickness and roughness. FESEM cross-sectional images of (A, B) TFG-EDA membrane, (D, E) TFG-DETA, and (G, H) TFG-TETA membrane. AFM images of (C) TFG-EDA, (F) TFG-DETA, and (I) TFG-TETA membranes.

S1.2.2 (b) Structural modelling of COF using Materials Studio.

The structural modelling of TFG-EDA, TFG-DETA, and TFG-TETA COFs was carried out using the Materials Studio 2020 software package (Accelrys Software Inc.).⁴ In the present study, the Primitive (P1) space group was used for all the eclipsed (AA) stacked mode of COF structures. The structures were optimized using the Forcite model with Universal force field before the refinement, and the refinement was done using the Pawley method with the experimental PXRD pattern using the Reflex module using previously reported studies.⁵ The 2-theta range was set from 2 to 40° with a step size of 0.02°. The structural refinement results are illustrated in **Figure 3(A-C)**, **Figure S13** and the final fractional atomic coordinates is summarised in **Table S1-S3**.

S1.3. Instrumentation and Methods

Fourier transform infrared (FT-IR) spectroscopy:

The FTIR spectra of the COF membranes were obtained using the Nicolet IR 6700 spectrometer (Thermo Fisher Scientific, USA) via the attenuated total reflectance (ATR) method.

Powder X-ray diffraction analysis and structural refinement:

The powder X-ray diffraction (PXRD) spectra of purified COF powder samples were obtained using the Rigaku Ultima instrument with a 2-40° range, with a step size of 0.02°.

X-ray photoelectron spectroscopy:

The surface elemental composition of the COF membranes was analyzed using the Thermofischer scientific Nexsa G2 X-Ray photoelectron spectrometer. XPS samples were prepared by mounting the COF film on a silicon wafer.

Small-angle X-ray scattering:

Small-angle X-ray scattering (SAXS) measurements were performed on the SAXS point 2.0 (Anton Parr) equipped with a Primux 100 micro microfocus Cu X-ray source. The sample-to-detector distance was kept at 1.07 m for analysis. A dense sample layer was packed in a powder cell for the SAXS analysis, and the measurements were done under vacuum at ca. 1 mbar. Using the SAXSanalysis 4.20 software, we converted the 2D scattering images into 1D radial intensity profiles (Anton Paar). The collected SAXS data were corrected for transmission, dark current, and background and averaged azimuthally as a function of the scattering vector q , where $q = 4\pi\lambda^{-1} \sin(\theta)$. The θ and λ are the scattering angle and the incident X-ray wavelength, respectively.

Atomic force microscopy:

The three-dimensional topography of COF membranes was measured with a hpAFM Asylum Research (MFP3D-BIO, Oxford Instruments, U.K.) in tapping mode, using a gold-coated silicon nitride tip. The COF film was carefully transferred to a silicon wafer, and a scratch was made with a sharp blade for measuring the thickness of the COF film at different interfacial polymerization times. For AFM-based nanoindentation experiments, a silicon-based AFM probe (ContAl-G) with resonant frequency of 13 kHz and a force constant of 0.2 N/m was used.

The force-displacement responses were recorded and examined during the approach and withdrawal stages.

Scanning/transmission electron microscopy

Scanning electron microscopy was performed using JSM-7800F (JEOL, Japan) instrument equipped with an EDS detector. The dried membranes were mounted on copper tape and coated with platinum for 60 s using a sputter coater. High-resolution transmission electron microscopy (HRTEM) was performed using a JEM-ARM200F NEOARM (JEOL, Japan) instrument with an accelerating voltage of 200 V. The dried samples were dispersed and mounted over a carbon-coated copper grid.

BET analysis

For the BET analysis, free-standing films (72 h) were fabricated, filtered, and repeatedly washed with DMAc, acetone, and ethanol. The dried film powder was further purified using a Soxhlet extractor with ethanol. Finally, N₂ adsorption/desorption analysis was performed using Autosorb iq4 (Quantachrome instruments). The sample was degassed at 437 K for 360 min, and the N₂ adsorption/desorption isotherm was collected at 77 K. The surface areas of COFs were determined by applying the Brunauer-Emmett-Teller (BET) model between P/P₀ values of 0.04 and 0.25. The related pore size distributions were calculated using the non-local density functional theory (NLDFT) method using the ASiQwin software.

Thermogravimetric analysis

Thermogravimetry analysis of COF samples were performed on a Thermal analyzer (TA instruments) with a ramp rate of 10 °C min⁻¹ from 25 °C to 750 °C to analyze their thermal stability.

Zeta potential

Zeta potential was measured to analyze the charge nature on the surface of COF membranes at different pH values ranging from 2 to 9. The measurements were performed on a Surpass 3 Electrokinetic analyzer (Anton Paar GmbH, Graz, Austria) using an adjustable gap cell.

Contact angle measurement

The surface wettability of COF membranes was analyzed by measuring the static water contact angle on a Drop shape analyzer DSA100 (KRÜSS GmbH, Germany) at ambient temperature.

Protein adsorption study

Protein adsorption onto COF membranes was studied using BSA as a model foulant in a phosphate-buffered saline (PBS, pH 7.4) solution. Briefly, a square piece of membrane (1 cm²) was immersed in the PBS solution and stirred gently for overnight. The soaked membranes were then dipped into a 1 mg mL⁻¹ BSA solution and shaken for 4 h at room temperature. Subsequently, the membranes were removed and thoroughly washed with fresh PBS. The BSA adsorption was quantified using a microplate reader (Synergy H1) to measure residual and wash solution using the Bradford Assay technique.² The BSA adsorption capacity was calculated using the following equation,

$$\text{BSA adsorption capacity } (\mu\text{g cm}^{-2}) = \frac{C_0 - C_f}{A} \quad (\text{S1})$$

where C_0 and C_f is the initial and final concentration of BSA. For direct visualization of protein on the membrane surface, an albumin–fluorescein isothiocyanate conjugate (FITC-BSA; Sigma Aldrich) adsorption test was performed. A FITC-BSA solution (0.05 mg mL⁻¹) was prepared in PBS (pH 7.4), and the membrane coupons were immersed and kept in the dark under gentle shaking conditions for 4 h. Subsequently, the membrane was removed and washed with fresh PBS solution. After that, the membrane was adhered to a microscopic glass slide, and fluorescence imaging was performed using a fluorescence microscope (Leica instruments).

Organic solvent nanofiltration performance and long-term OSN performance

Organic solvent nanofiltration (OSN) experiments were performed using a stainless-steel dead-end filtration set up with an effective filtration area of 15.18 cm². The operational pressure was controlled by using a N₂ gas cylinder, and all the filtration performances were conducted under ambient conditions. Prior to interfacial polymerization, the support PET membranes were cut to match the diameter of the filtration area, and the interfacial films were transferred onto the support membrane surface. Pure water and organic solvent permeance (L m⁻² h⁻¹ bar⁻¹) were measured with various solvents, including methanol, ethanol, isopropanol, hexane, DMF, and

acetone. All permeation data were calculated after achieving steady-state filtration, typically after 30 min of filtration. The pure solvent flux was calculated using the following equation:

$$\text{Solvent permeance } (L m^{-2} h^{-1} bar^{-1}) = V_p / A_m \Delta t \Delta p \quad (S2)$$

where, V_p is the permeation volume, A_m is the effective membrane area, Δt is the filtration time, and Δp is the applied nitrogen pressure.

After solvent permeation studies, the reservoir was filled with different dye solutions to evaluate the dye rejection performance of COF membranes. In our study, we used 4-nitrophenol, Methylene blue, orange G, Rhodamine B, Congo red, and Brilliant blue dyes. Finally, the test solution was filtered through the membrane, and the permeates and retentates were collected to quantify the rejection performance. The solute rejection percentage was calculated using the given equation:

$$\text{Solute rejection } (\%) = \left(1 - \frac{C_p}{C_f}\right) \times 100 \quad (S3)$$

where, C_p and C_f is the permeate and feed concentration of dye. The feed, retentate, and permeate concentrations were measured using a UV-visible spectrophotometer. Unless specified, all the OSN experiments were carried out at least three to four times for individual samples.

The molecular weight cut-off (MWCO) of COF membranes was determined using neutral PEG molecules of different molecular weights (200, 400, 600, 800, 1000, and 2000 Da) in water (0.5 g L^{-1}). After the filtration test, the filtrates were collected and treated with a 5% $BaCl_2$ solution and a 0.05 M iodine solution. The UV absorbance of the treated filtrates was quantified at 590 nm using a microplate reader (Synergy H1, Biotek, USA), and the concentration of PEG was determined with a standard curve comprised of PEGs that were identical to the PEGs being measured. The percentage of rejection was calculated using **equation S3**. The PEG rejection data were further used to evaluate the pore size and the pore size distribution of the COF membranes. The relationship between Stokes diameter (D_p) and molecular weight (M_w) of PEG solute is given below.³

$$\text{Stoke diameter } (D_p) = 33.46 \times 10^{-12} \times M_w^{0.557} \quad (S4)$$

Additionally, a lognormal distribution curve was produced in order to acquire the pore size distribution of membranes based on the PEG rejection data. The following probability density

function equation can be used to estimate the pore size distribution and the mean pore diameter (equation S5):

$$\frac{dR(r_p)}{dr_p} = \frac{1}{\sqrt{2\pi} r_p \ln\sigma_p} \exp\left\{-\frac{(\ln r_p - \ln\mu_p)^2}{2(\ln\sigma_p)^2}\right\} \quad (\text{S5})$$

where, μ_p is the mean pore effective pore size, and σ_p is the geometrical standard deviation which can be calculated by dividing the rejection ratio at 84.13% and 50%. Similarly, BSA rejection was done to evaluate the antifouling performance of membranes.

Dynamic membrane fouling

To antifouling performance of COF membranes was evaluated by filtering a BSA solution (in PBS at pH 7.4, g mg/mL) in three steps: pure water filtration (J_{wi}), BSA filtration (J_{BSA}), and filtration of pure water after BSA filtration (J_{wr}). After the BSA filtration test, the membranes were rinsed with pure water to check the flux recovery using the following equation:

$$\text{flux recovery (\%)} = \frac{J_{wf}}{J_{wi}} \times 100 \quad (\text{S6})$$

Furthermore, the reversible fouling and irreversible fouling were calculated to understand the antifouling mechanisms using the following equations,

$$\text{Reversible fouling (R}_r\text{)} = \frac{J_{wr} - J_{BSA}}{J_{wi}} \quad (\text{S7})$$

$$\text{Irreversible fouling (R}_{ir}\text{)} = \frac{J_{wi} - J_{wr}}{J_{wi}} \quad (\text{S8})$$

where J_{wi} is the initial flux, J_{wr} is the recovered flux, and J_{BSA} is the flux during BSA filtration

S2: Solid state ^{13}C NMR of TFG-EDA, TFG-DETA, and TFG-TETA

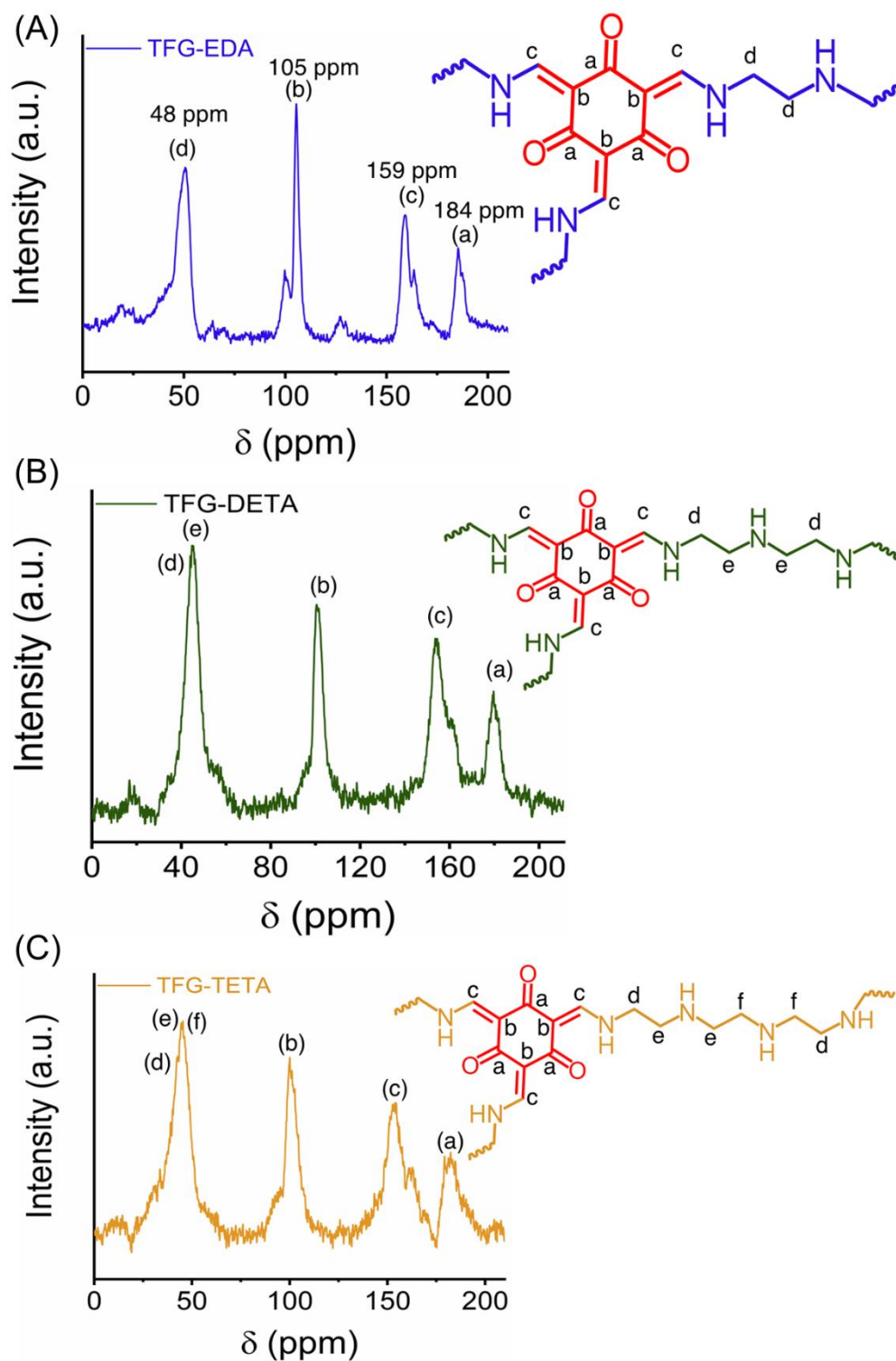


Figure S4 | ^{13}C CP-MAS spectra of (A) TFG-EDA, (B) TFG-DETA, and (C) TFG-TETA COFs.

S3: Morphological analysis

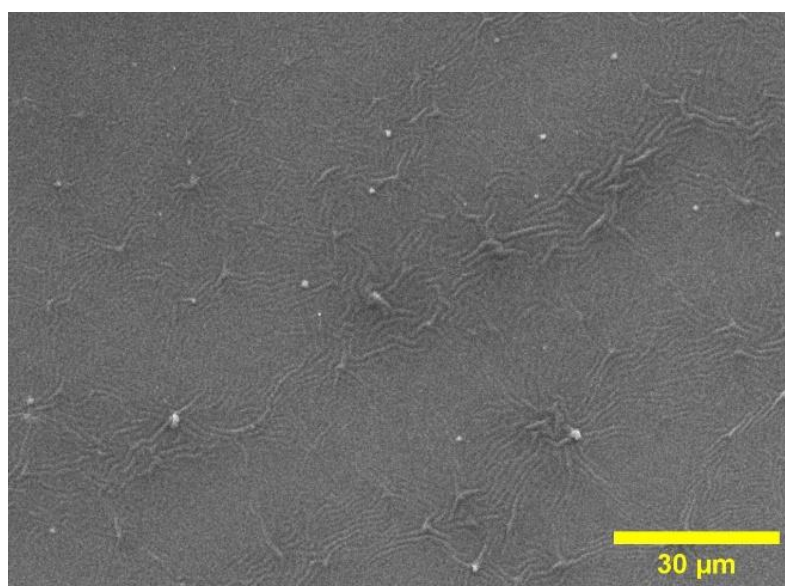


Figure S5| Low magnification FESEM image of large area TFG-EDA membrane.

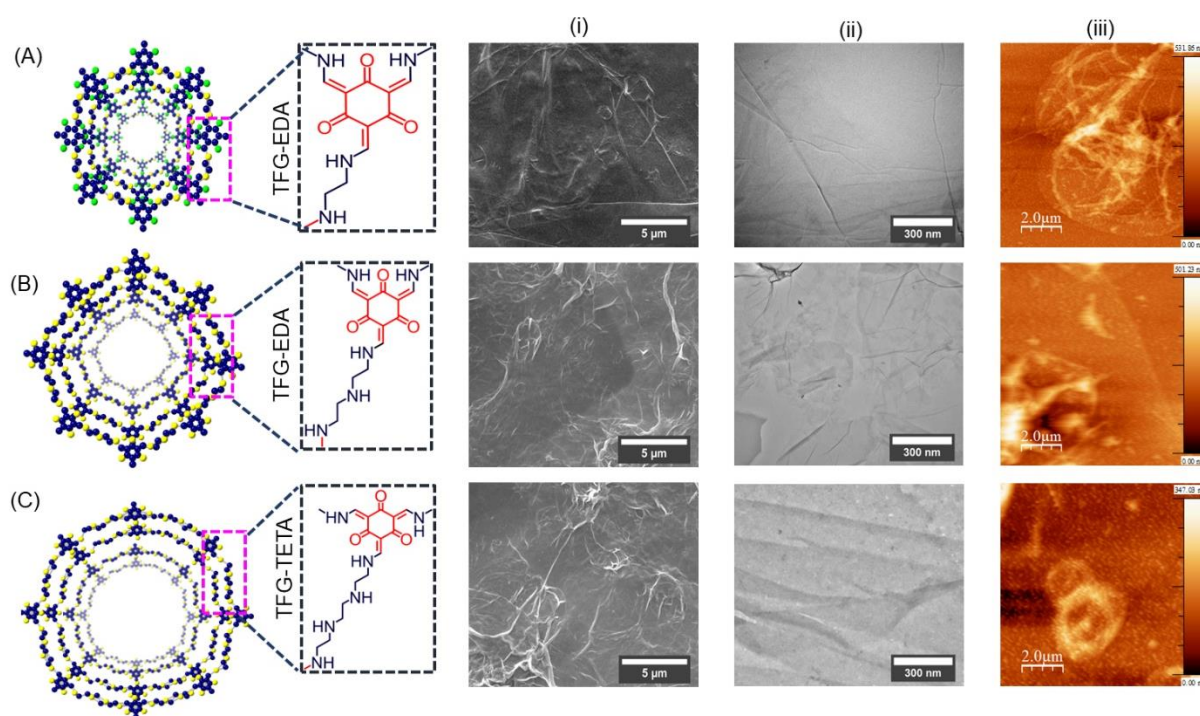


Figure S6| Characterization of COF membranes. Schematic structure of synthesized COF structures (A) TFG-EDA, (B) TFG-DETA, (C) TFG-TETA, (i) FESEM, (ii) TEM, and (iii) AFM images of the corresponding COF membranes.

S4: FTIR of COF membranes

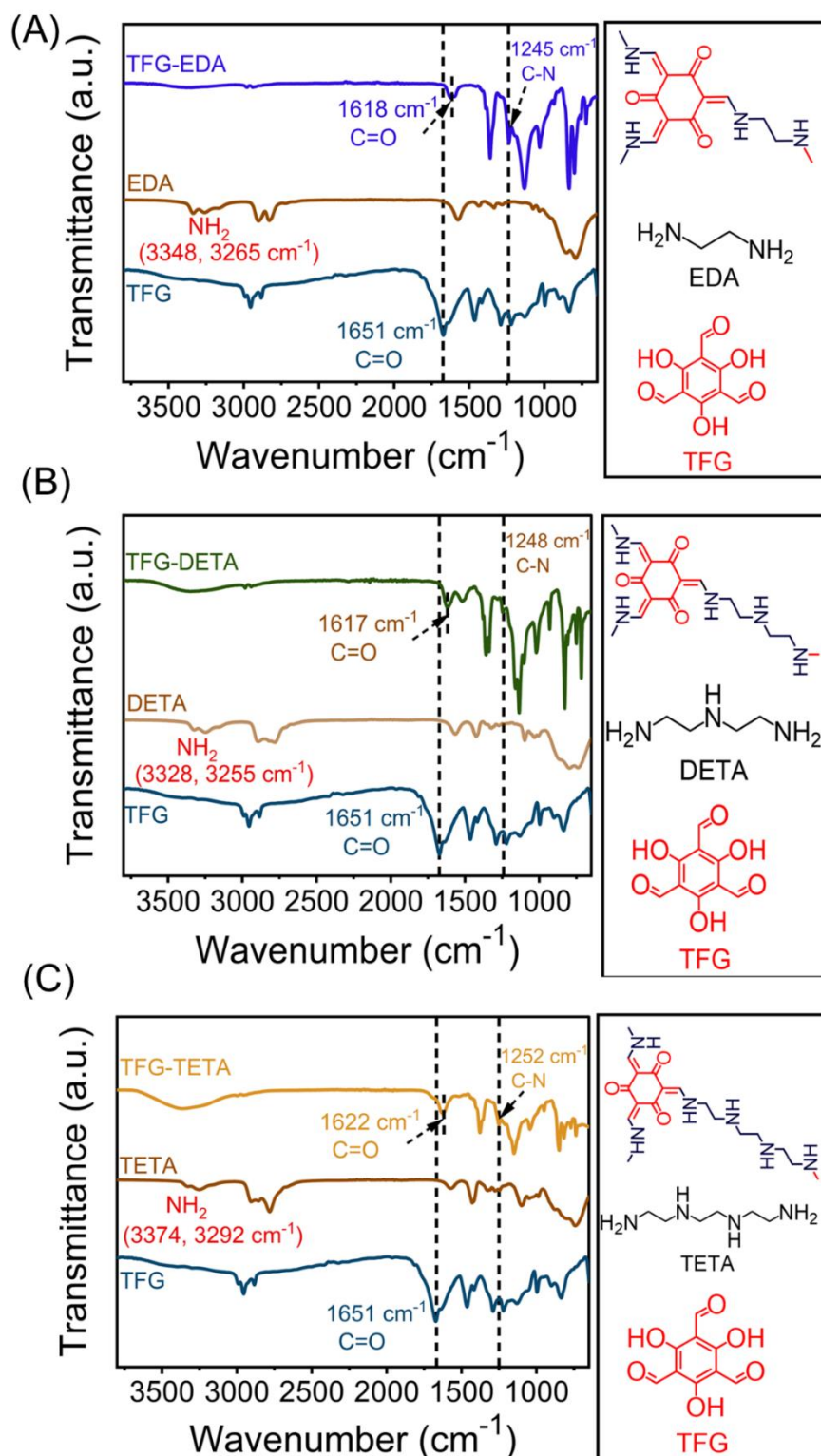


Figure S7 | FTIR spectra of interfacially crystallized COF membranes (A) TFG-EDA, (B) TFG-DETA, and (C) TFG-TETA.

S5. X-Ray photoelectron spectroscopy analysis

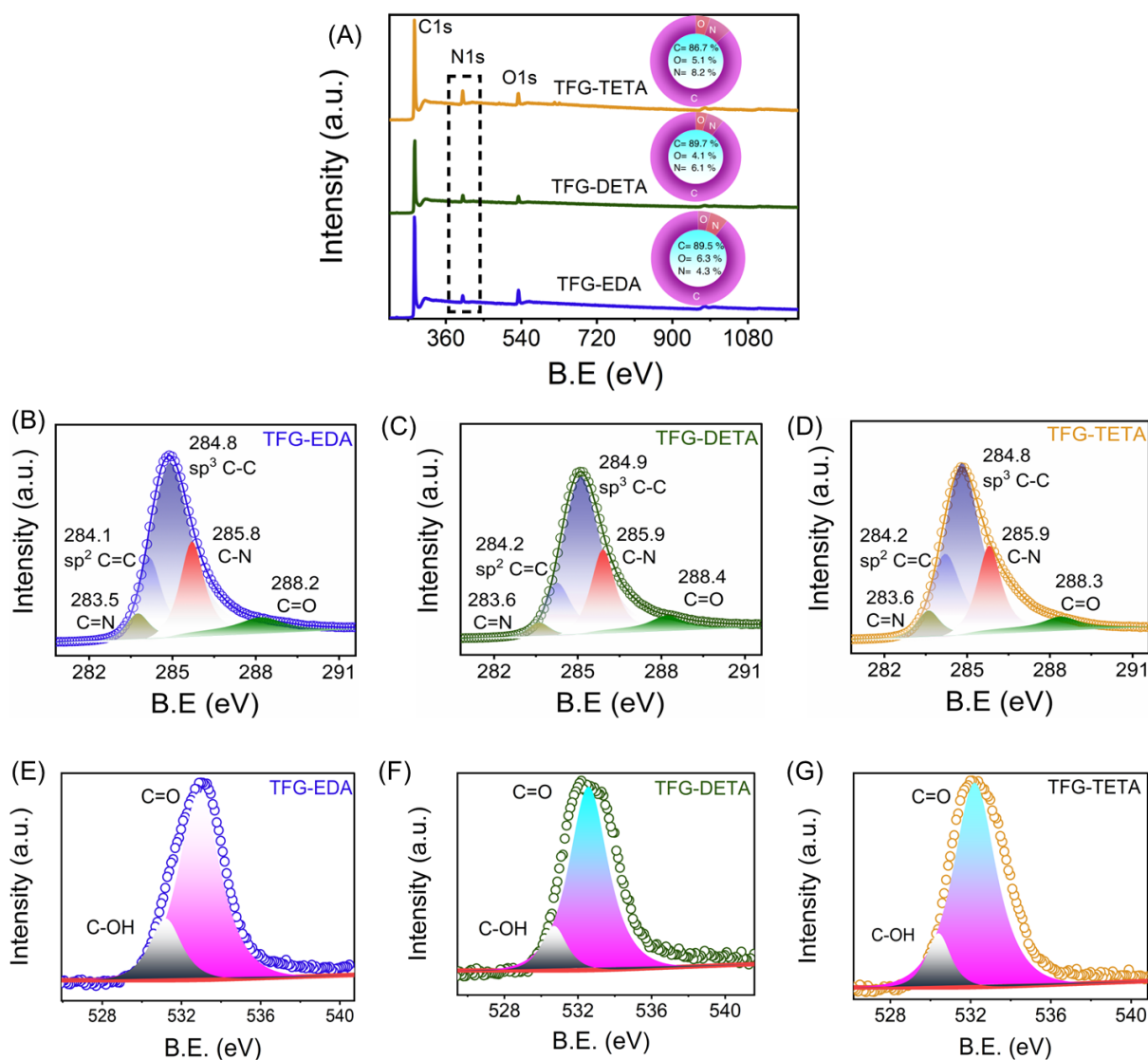


Figure S8 | High-resolution X-ray photoelectron spectra of COF membrane, (A) survey spectra (inset pie chart shows the elemental composition), (B-D) deconvoluted C1s spectra, (E-G) deconvoluted O1s spectra of TFG-EDA, TFG-DETA, and TFG-TETA.

S6: BET summary

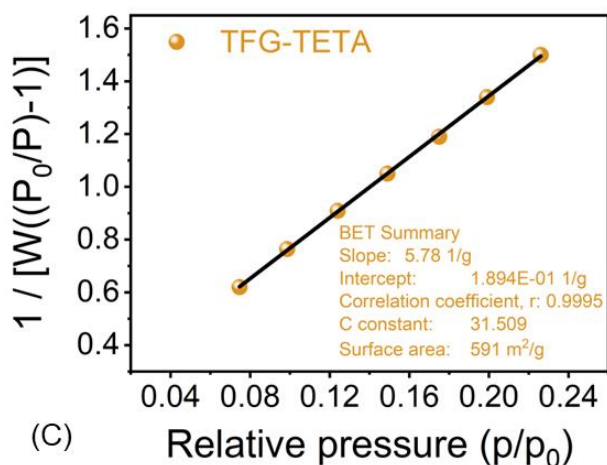
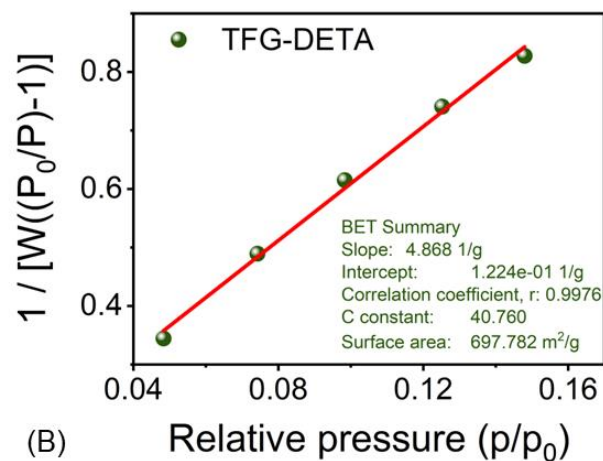
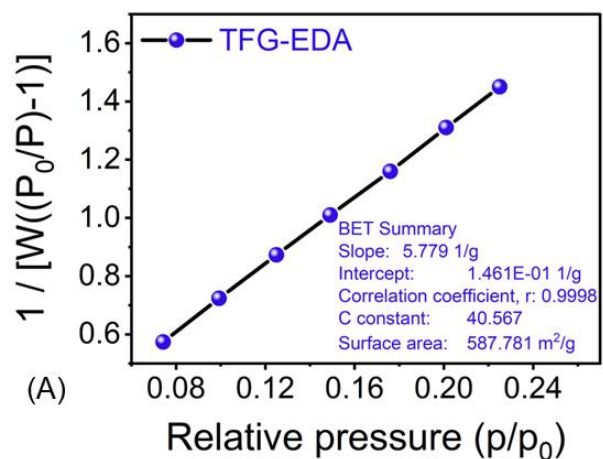


Figure S9 | Plots of the linear region for the BET equation for (A) TFG-EDA, (B) TFG-DETA, and (C) TFG-TETA.

S7. TGA analysis

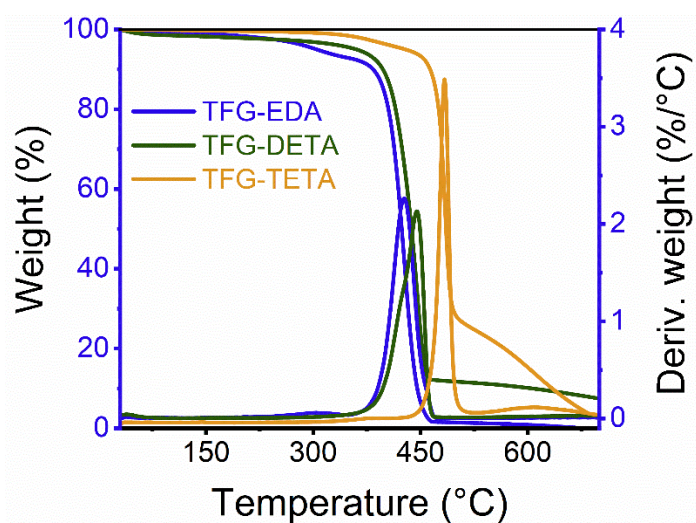


Figure S10 | Thermogravimetry analysis of TFG-EDA, TFG-DETA, and TFG-TETA thin films

S8: PXRD of COF membrane

S8.1: PXRD of COF membrane over the support

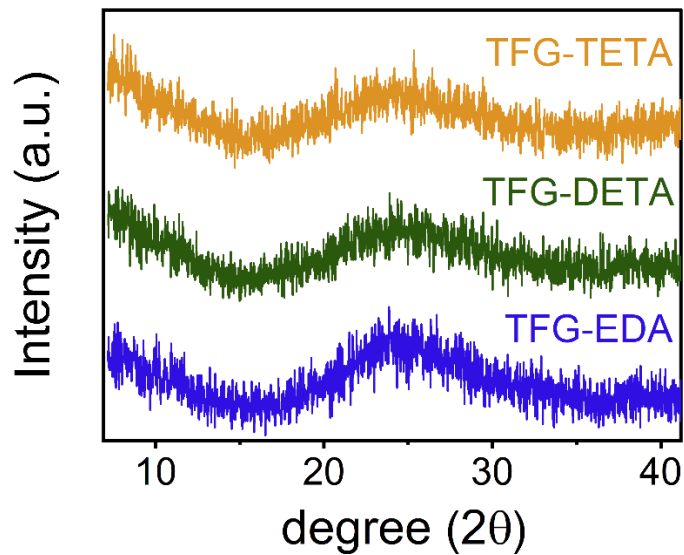


Figure S11 | XRD of COF films obtained after interfacial polymerization of 120 min

S8.2. Effect of interfacial polymerization time on crystallinity

To study the effect of interfacial polymerization time on the COF crystallization process, we performed the XRD at different polymerization times. We observed a broadening in XRD spectra when the COF membrane mounted over polymeric support as the polymeric supports peak mainly interfered with the COF spectra. Therefore, we have collected the XRD spectra by mounting the COF membrane sample over a zero background sample holder (Malvern Panalytical). This requires minimal sample quantity and provides a better XRD pattern without background interference. From the XRD spectra, it can be postulated that the formation of a well-crystalline COF predominantly depends on the polymerization time. No noticeable PXRD spectra were detected in the initial phase of polymerization up to 60 min. However, after 120 min of interfacial polymerization, the XRD pattern demonstrated two diffraction peaks at $\sim 3.7^\circ$ and 26° , corresponding to (100) and (001) reflection planes from the COF, confirming the formation of crystalline COF at the interface.

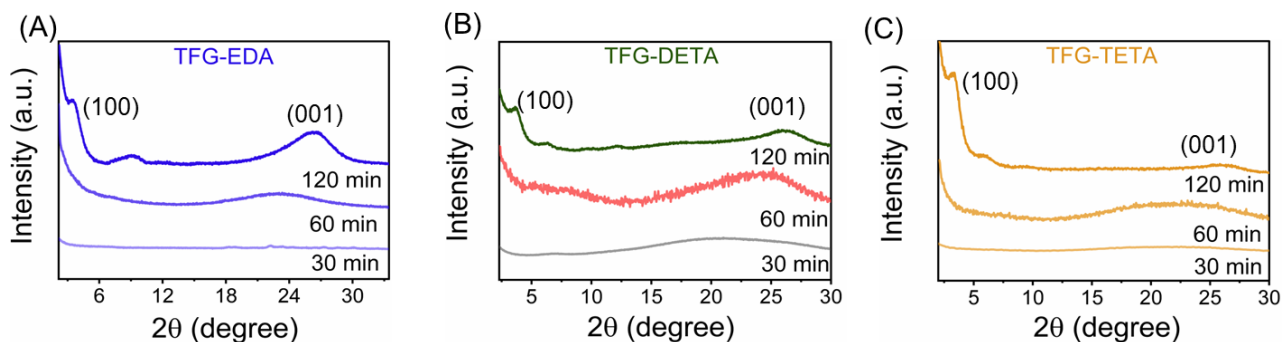


Figure S12 XRD spectra of (A) TFG-EDA, (B) TFG-DETA, and (C) TFG-TETA COF films obtained at different interfacial polymerization times.

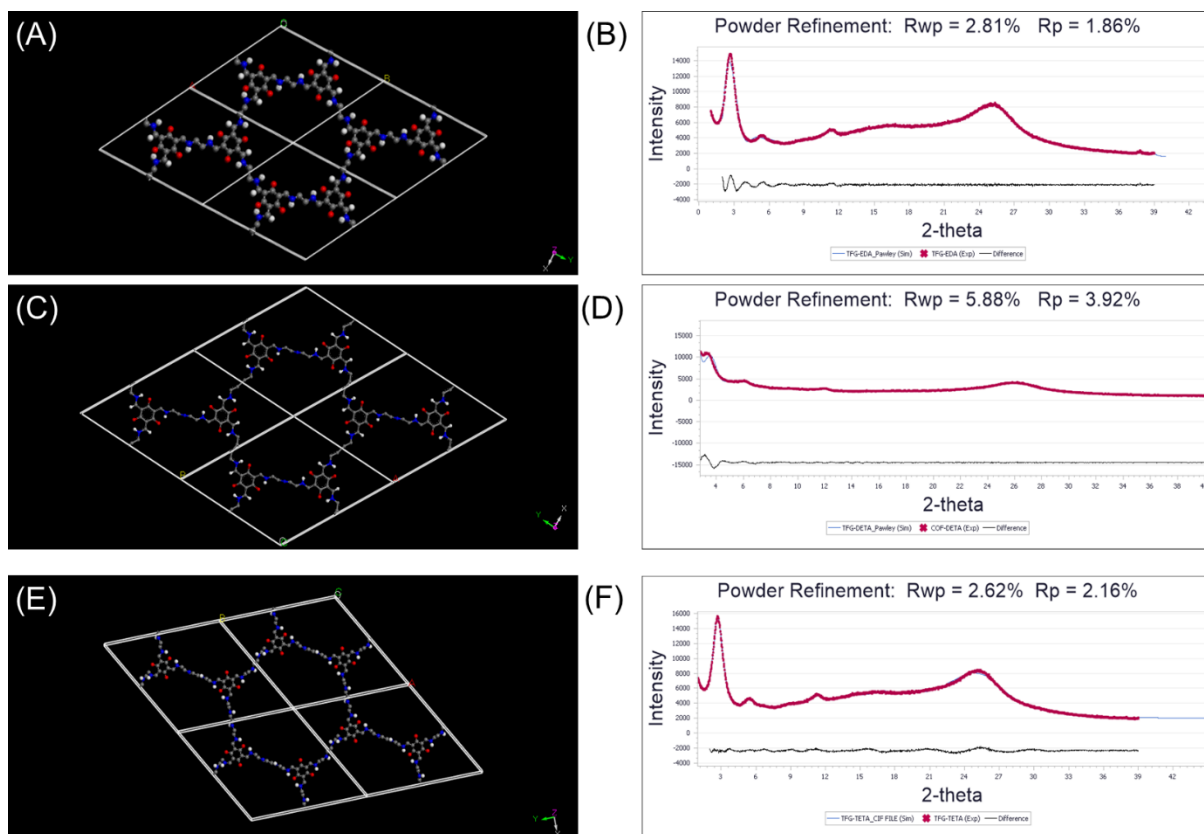


Figure S13 Eclipsed crystal lattice packing of (A)TFG-EDA, (C)TFG-DETA (E)TFG-TETA and PXRD refinement using Pawley method of (B)TFG-EDA, (D)TFG-DETA and (F)TFG-TETA membranes.

S9: Static BSA adsorption test

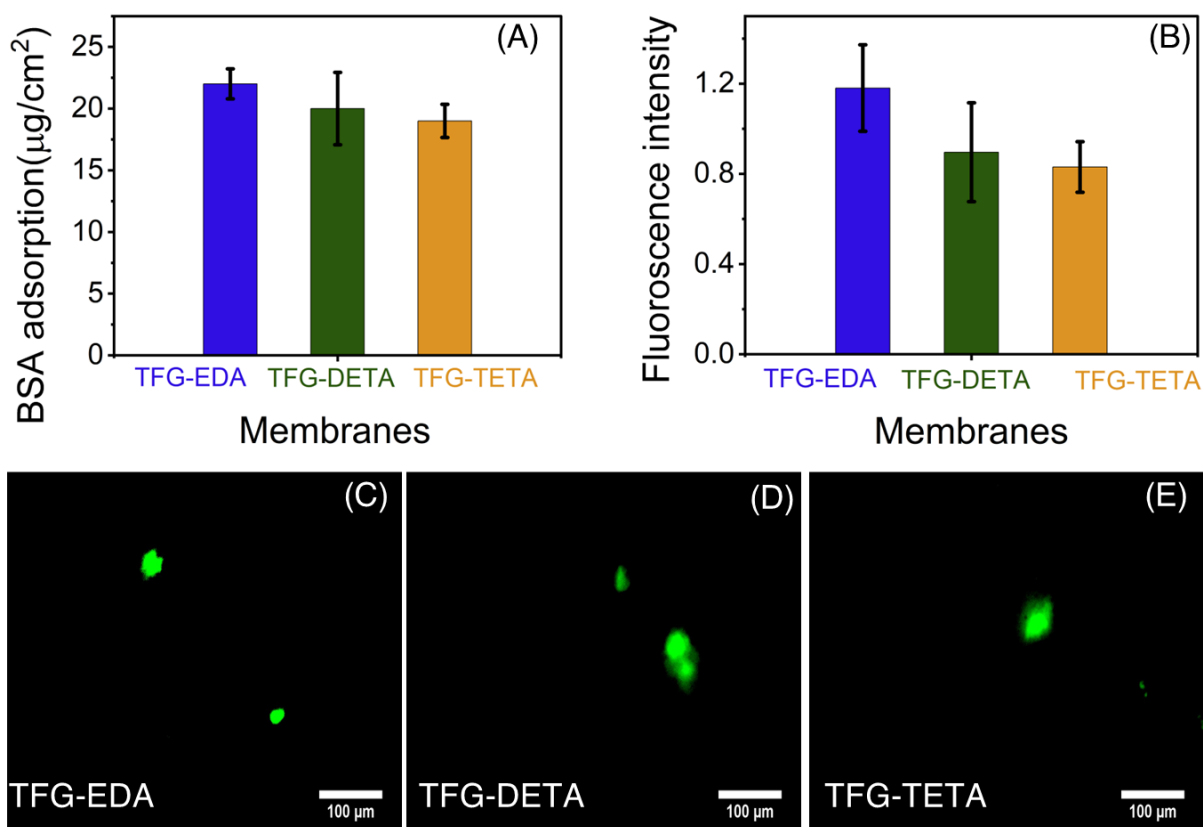


Figure S14 | (A) static BSA adsorption, (B) fluorescence intensity of FITC-BSA adsorbed on the membrane surface, (C-E) Fluorescence images of adsorbed FITC-BSA on different membranes.

S10: Additional information about Atomic force microscopy

COFs are a class of crystalline porous materials in which the individual linkers are covalently bonded, making the COF membranes mechanically stable. To elucidate the nanomechanical properties of interracially crystallized COF thin films, we have performed AFM-based nanoindentation experiments by transferring the COF-x films with a thickness of ~ 105 nm onto a cleaned Si wafer. Prior to indenting, the COF thin films were scanned in noncontact mode, and the tip was placed on a smoother surface. During the AFM nanoindentation experiment, we applied force on the tip and allowed for the nano penetration of the tip on the film's surface, subsequently measuring how the sample responded as a function of indentation. In general, the behavior of a polymer sample during a nanoindentation experiment is represented schematically in **Figure S15 (Supp. Info.)**. Typically, DMT (Derjaguin–Muller–

Toporov) and JKR (Johnson–Kendall–Roberts) models are used to calculate the elastic modulus when adhesion occurs between the sample and tip surface.⁴ The JKR model accounts for adhesion forces within the contact area, whereas the DMT model considers adhesive forces away from the contact area.⁵ Hence, the JKR model may be more appropriate for calculating the modulus for a sample displaying strong adhesive properties. The JKR model calculates the modulus using locations on the unloading portions of the force-separation curve. The elastic modulus of the COF membrane was calculated using the following equation,

$$E = \frac{3}{4} (1 - \nu^2) \left(\frac{1+16\frac{1}{3}}{3} \right)^{3/2} \frac{F_a}{(R(d_0-d_1)^3)^{1/2}} \quad (\text{S9})$$

there the ν is the Poisson's ratio (0.27), R is the tip radius (10 nm), and the values of F_a , d_0 and d_1 can be obtained from the force-displacement curve (**Figure S15**).

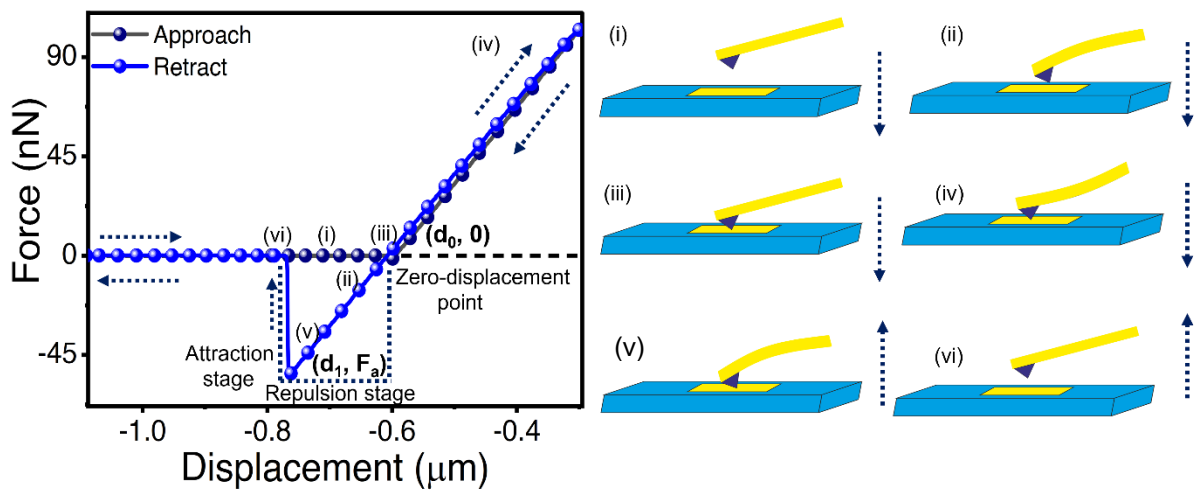


Figure S15 | Force versus displacement graphs show an approach and retract curve for TFG-DETA membrane, and the schematics represent the relative positions of the tip and the sample during different stages of the AFM nanoindentation process. Initially, the AFM tip was positioned at a longer distance from the sample surface. Subsequently, the tip was moved towards the sample surface (I) from the initial position, and this movement measured the gradual increase in negative force (adhesion). When the adhesion approaches its local maximum, a sudden jump in the phenomenon can be observed at a certain displacement value (II). This jump can be attributed to the bending of the AFM cantilever towards the sample surface during maximal adhesion. Eventually, the cantilever bending towards the sample reduces within displacement until there is an absence of negative load. This point corresponds to the zero displacement point, which assures a strong tip-to-surface contact (III), and the

indentation stage begins from this point (IV). When the cantilever bends away from the sample surface during the indentation phase, the tip experiences a positive force.

S11. Molecular weight cut-off analysis

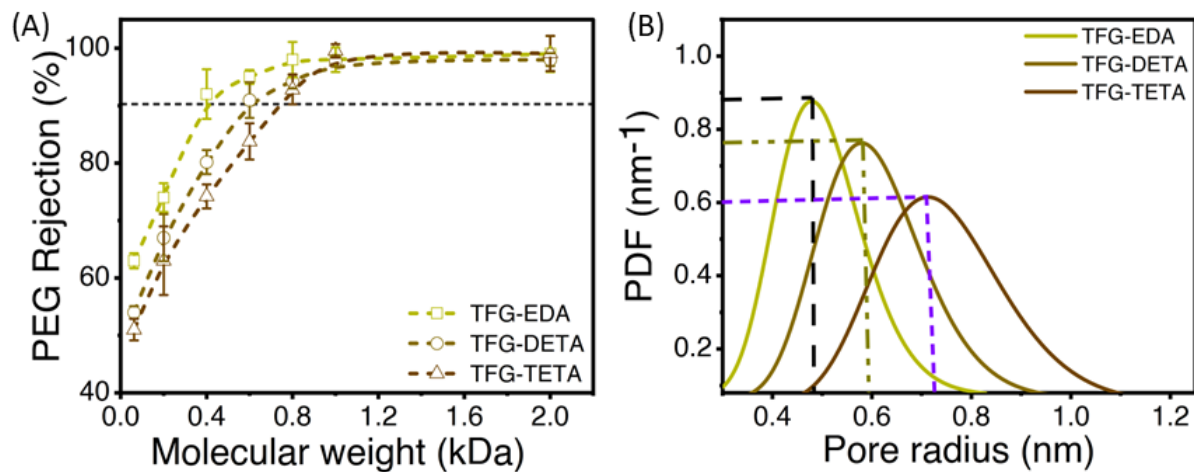


Figure S16 (A) Rejection of different molecular weight PEG by different COF membranes, and (B) log-normal plot for pore size distribution.

S12: Additional information for OSN performance

S12.1. Stability test of COF membranes

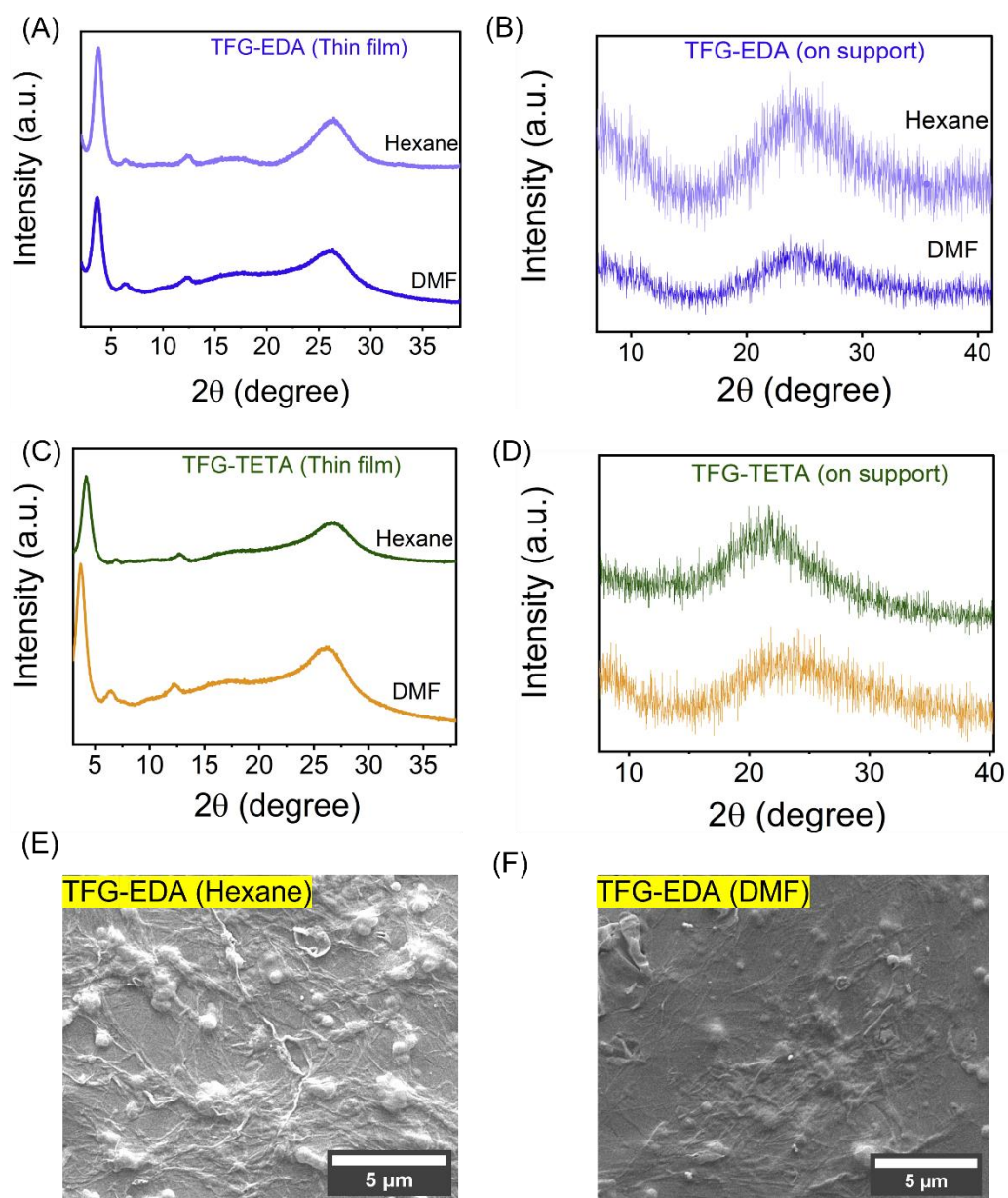


Figure S17 | Stability test of COF thin films or membranes under polar (DMF) and nonpolar (hexane) solvent. The COF membranes were immersed in the solvents for 48 h, followed by drying under vacuum before the characterization.

S12.2: Effect of COF layer thickness on solvent flux

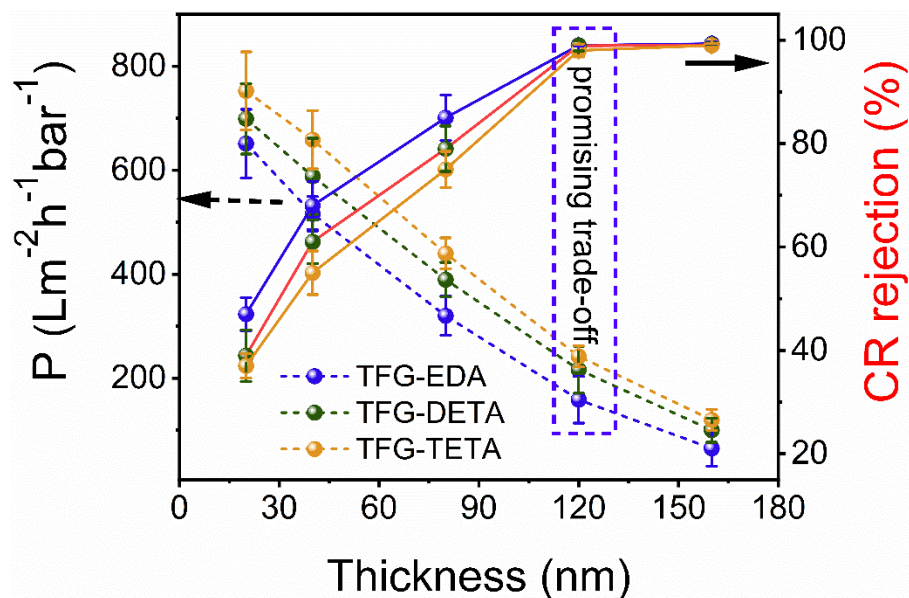


Figure S18 Effect of COF layer thickness on the pure water permeance and Congo red (CR) rejection.

S12.3: Effect of pressure on water flux and membrane morphology after filtration

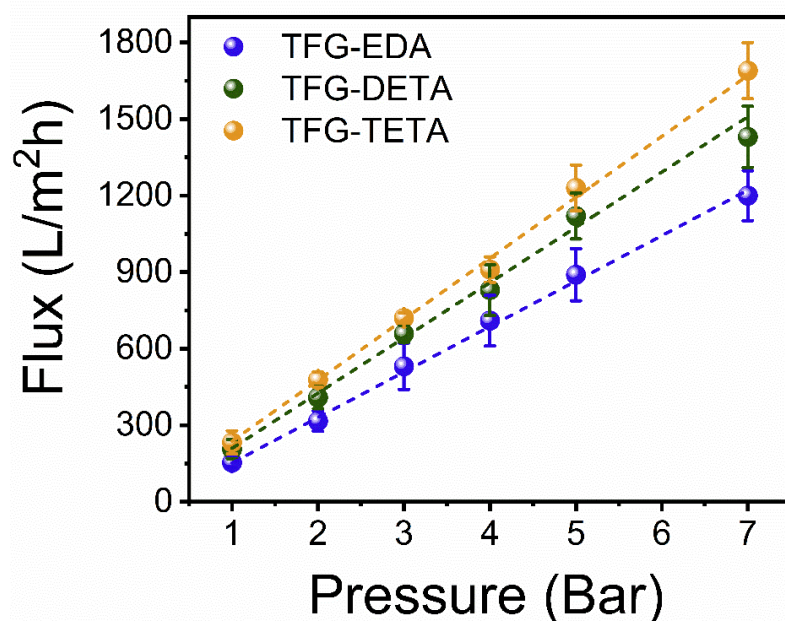


Figure S19 Effect of pressure on water flux through COF membranes.

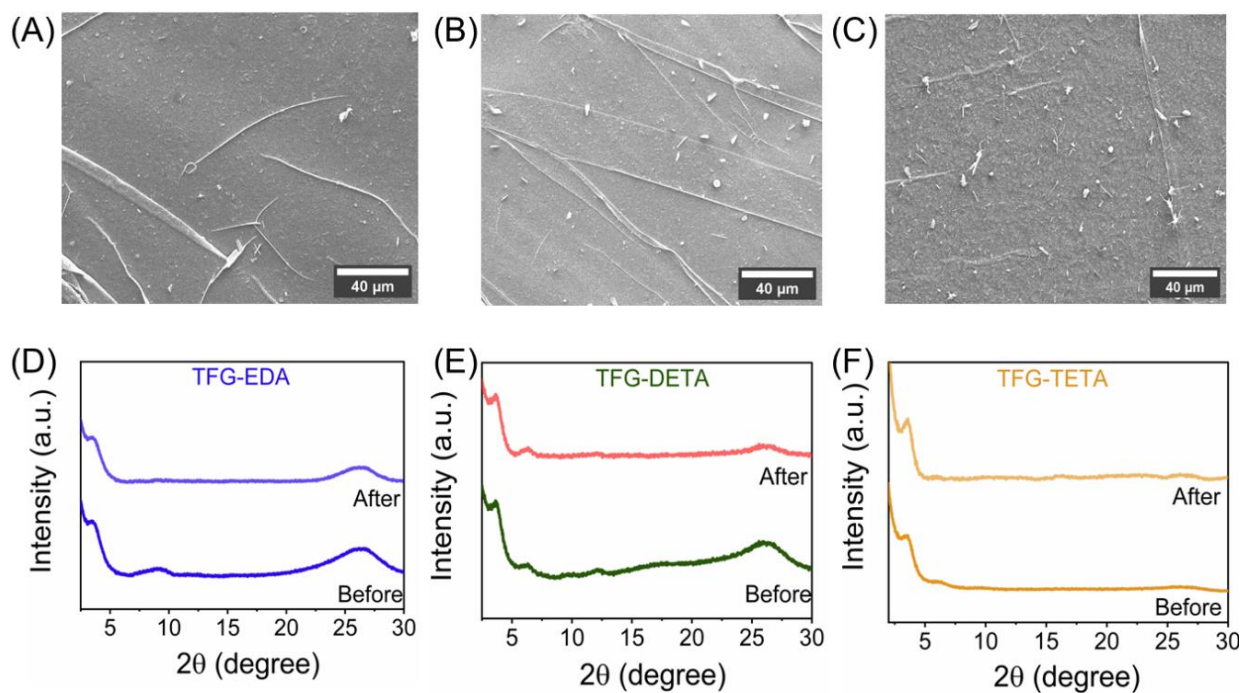


Figure S20 | FESEM images and PXRD spectra after pressure-dependent filtration test (A) TFG-EDA, (B) TFG-DETA, and (C) TFG-TETA. (low magnification images were taken to visualize the surface phenomenon over a large area), (D-F) PXRD spectra of COF film before and after pressure filtration test.

S12.2: Effect of pressure on solvent flux

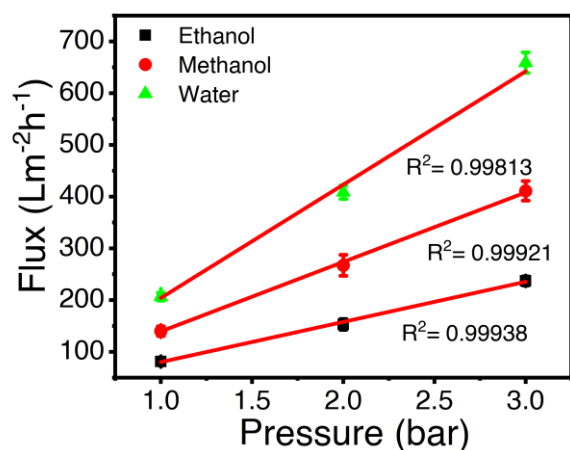


Figure S21 | Solvent flux as a function of applied pressure for TFG-DETA membrane.

S12.3: Plots of permeances of different solvents of COF membranes based on different models

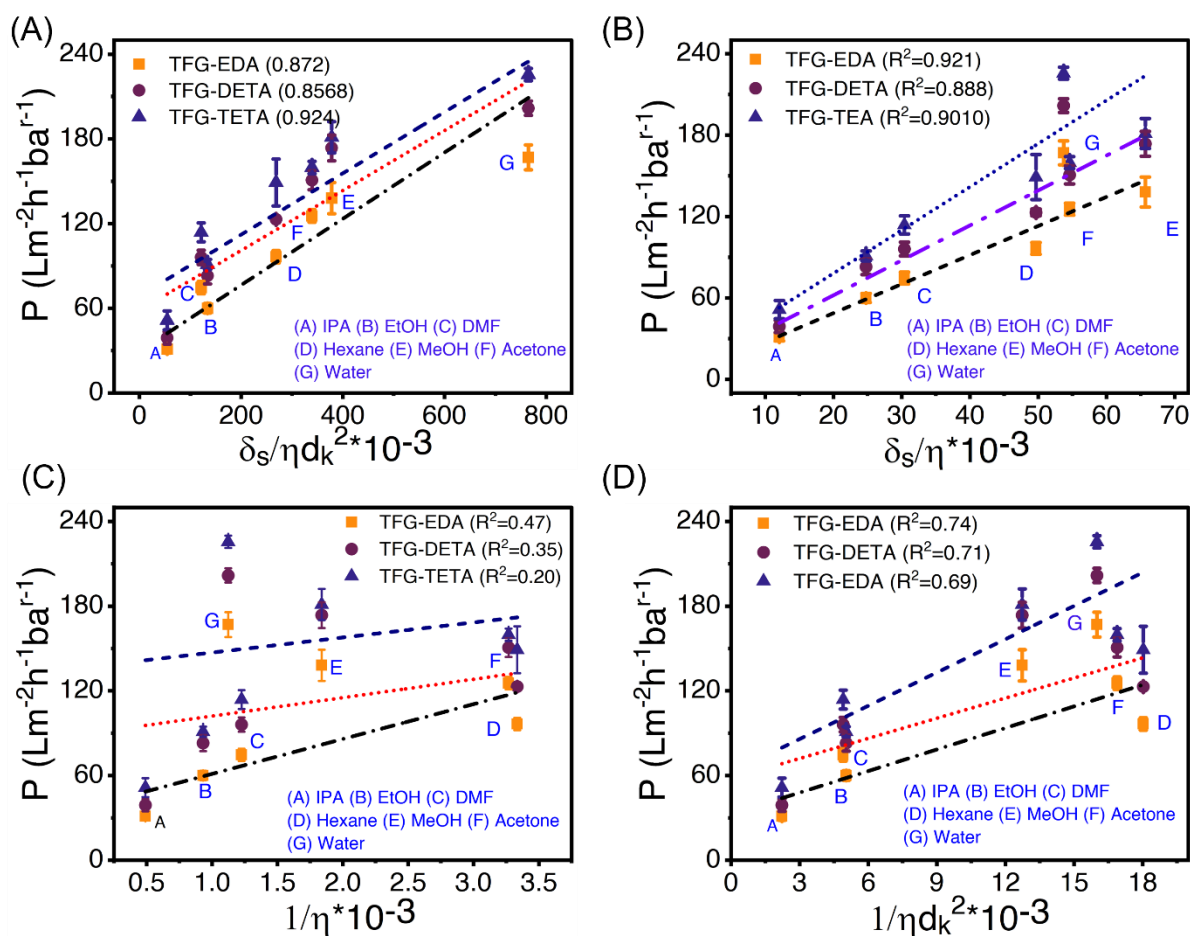


Figure S22 | Plots of permeances of different solvents of COF membrane based on different models: (A) permeance versus solvent viscosity (η) and total Hansen solubility parameter (δ_s); (B) permeance versus solvent viscosity (η), kinetic diameter (d_k) and total Hansen solubility parameter (δ_s); (C) permeance versus solvent viscosity (η); (D) permeance versus solvent viscosity (η) and kinetic diameter (d_k).

S12.4: UV-vis absorbance changes of retentate of Congo red solution

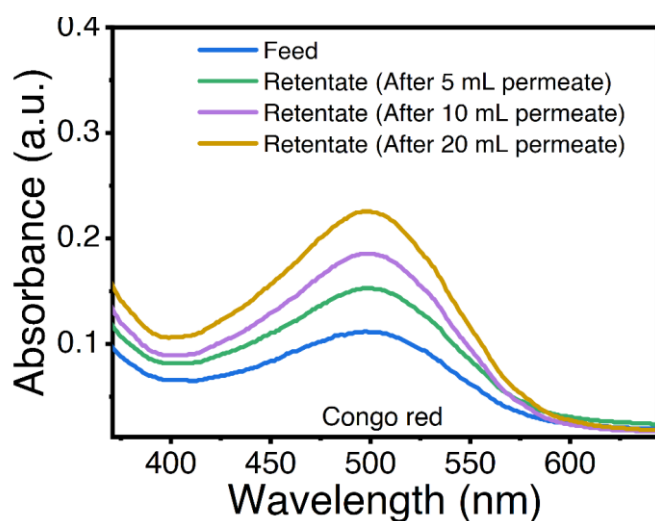


Figure S23 | UV-vis absorbance changes of retentate of Congo red solution when the permeation volume was 5, 10 and 20 mL.

S12.5: Permeance and rejection performance of Rhodamine-B and Orange-G

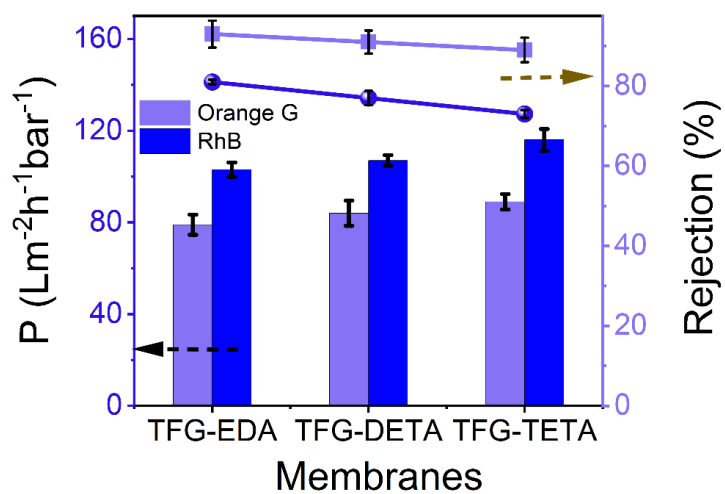


Figure S24 | Permeance and rejection performance of Rhodamine-B (RhB) and Orange-G by COF membranes

S12.6: Uv-visible spectra after molecular rejection experiment

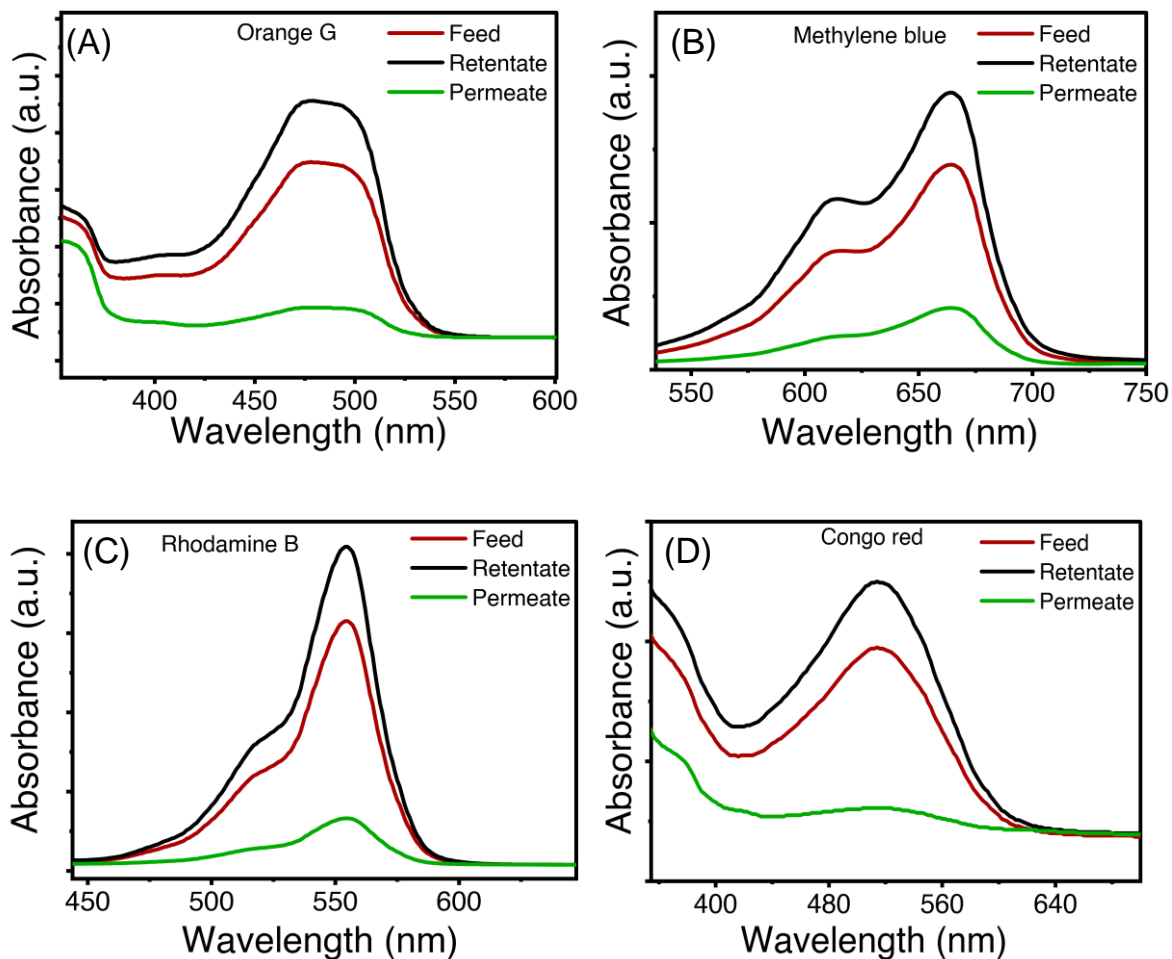


Figure S25 | Uv-visible spectra of feed, retentate and permeate after molecular separation performance by TFG-DETA membrane.

S12.7. Long-term dye rejection performance of COF membranes

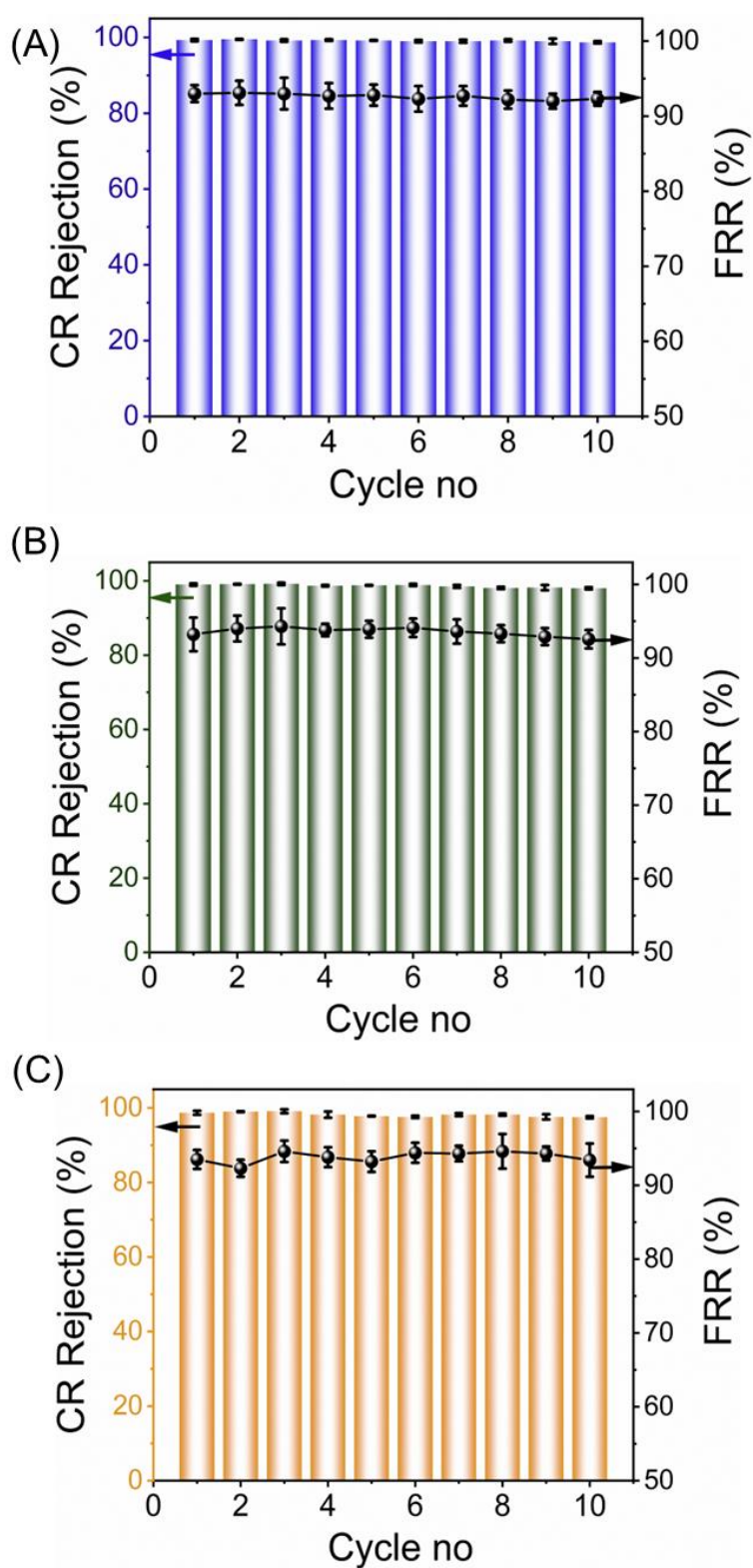


Figure S26 | Recyclability of COF membranes towards Congo red (CR) rejection and Flux recovery (A) TFG-EDA, (B) TFG-DETA, and (C) TFG-TETA membranes.

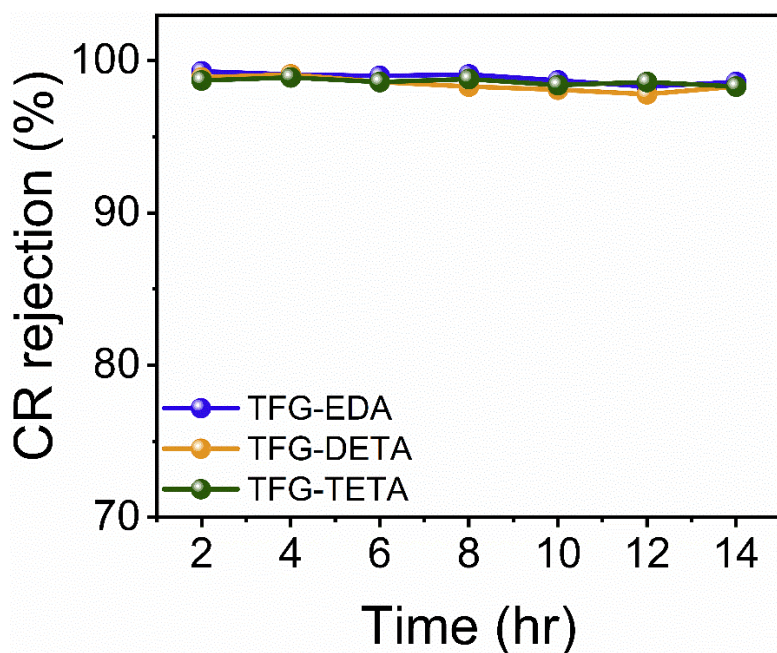


Figure S27 | Long-term dye (Congo red) rejection performance on the COF membranes

S13: Dynamic antifouling performance

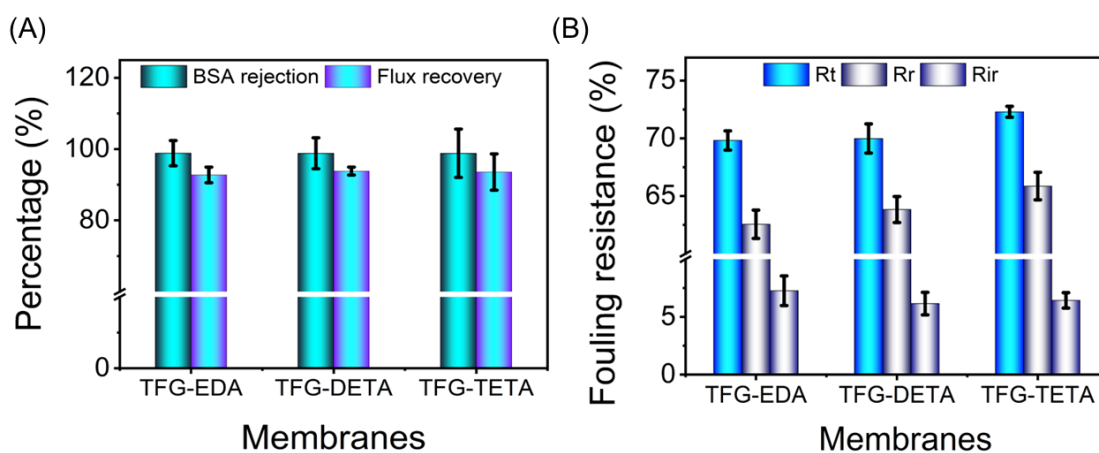


Figure S28 | Dynamic BSA fouling experiments of COF membranes, (A) BSA rejection and flux recovery of COF membranes, (B) reversible (R_r), irreversible (R_{ir}), and total (R_t) fouling on membranes during BSA filtration.

S13: Structural Modelling and refinement of COFs

Table S1: Fractional atomic coordinates for the unit cell of TFG-EDA

Space group P1, a = 19.78 Å, b = 30.54 Å, c = 3.53 Å, α = 92.08°, β = 92.02°, and γ = 121.59°			
Pawley refinement Rp = 1.86%, Rwp = 2.81%			
Atom	X(Å)	Y(Å)	Z(Å)
O1	0.30734	0.53018	0.76599
N2	0.46638	0.57492	0.79547
C3	0.32852	0.60749	0.78443
C4	0.41666	0.66951	0.80975
C5	0.48389	0.65213	0.81562
C6	0.53373	0.55995	0.804
H7	0.40393	0.52897	0.77408
O8	0.52325	0.81006	0.85382
N9	0.46985	0.91221	0.87191
C10	0.43735	0.74903	0.82945
C11	0.36997	0.76577	0.82341
C12	0.38673	0.84431	0.84283
C13	0.47904	0.98657	0.88994
H14	0.52326	0.90779	0.8801
O15	0.21634	0.71823	0.79104
N16	0.10242	0.56756	0.74214
C17	0.28201	0.70238	0.79729
C18	0.2611	0.62338	0.77794
C19	0.17362	0.55853	0.75139
C20	0.01868	0.50092	0.7145
H21	0.11125	0.62215	0.75507
O22	0.73396	0.50852	0.84527
N23	0.57504	0.46393	0.7919
C24	0.71274	0.43121	0.82009
C25	0.62461	0.36926	0.78322
C26	0.55744	0.3867	0.77085

C27	0.50776	0.47898	0.78103
H28	0.63751	0.50983	0.81522
O29	0.51797	0.22874	0.72258
N30	0.57085	0.12647	0.71355
C31	0.60389	0.28975	0.75869
C32	0.67118	0.27293	0.77125
C33	0.65413	0.19426	0.74869
C34	0.56135	0.05197	0.69446
H35	0.51756	0.13108	0.70169
O36	0.82494	0.32046	0.81923
N37	0.93923	0.47212	0.88029
C38	0.75922	0.3363	0.80739
C39	0.78015	0.41534	0.83172
C40	0.86754	0.48045	0.86762
C41	1.02272	0.53927	0.9139
H42	0.93094	0.41773	0.8647
H43	0.16238	0.50166	0.738
H44	0.33349	0.85129	0.83543
H45	0.87831	0.53716	0.88471
H46	0.70723	0.18709	0.75952

Table S2: Fractional atomic coordinates for the unit cell of TFG-DETA

Space group P1, a = 25.05 Å, b = 28.24 Å, c = 3.57 Å, α = 85.9°, β = 84.27°, and γ = 110.7°			
Pawley refinement Rp = 3.92%, Rwp = 5.88%			
Atom	X(Å)	Y(Å)	Z(Å)
O1	0.29057	0.4978	0.9557
N2	0.40676	0.52812	0.86435
C3	0.29672	0.55302	0.94331
C4	0.3561	0.59458	0.94933
C5	0.40932	0.57973	0.96591
C6	0.45214	0.50769	0.96452

H7	0.37119	0.50499	0.71646
O8	0.42086	0.69096	0.9498
N9	0.37285	0.76414	0.87629
C10	0.36227	0.65083	0.9418
C11	0.30892	0.66565	0.92325
C12	0.31461	0.72208	0.89877
C13	0.37758	0.81912	0.84746
H14	0.41225	0.75487	0.87847
O15	0.19701	0.63865	0.9151
N16	0.12936	0.536	0.9613
C17	0.24921	0.62382	0.9258
C18	0.24316	0.56743	0.93572
C19	0.18396	0.52473	0.94202
C20	0.07206	0.49301	0.97946
H21	0.13096	0.57565	0.96652
O22	0.6638	0.35119	0.95409
N23	0.54757	0.32184	0.94466
C24	0.6572	0.29604	0.9434
C25	0.59687	0.25408	1.00704
C26	0.54322	0.26845	1.07405
H27	0.58687	0.34824	0.76283
O28	0.53049	0.15729	1.06197
N29	0.57938	0.08535	0.95716
C30	0.59003	0.19786	1.00039
C31	0.64378	0.18357	0.92335
C32	0.63791	0.12758	0.90358
C33	0.57472	0.03088	0.93609
H34	0.53981	0.09418	1.0117
O35	0.75655	0.21113	0.78994
N36	0.82525	0.31262	0.77025
C37	0.70423	0.22557	0.86311
C38	0.71102	0.28189	0.87616

C39	0.77102	0.32461	0.82516
C40	0.88332	0.35527	0.72604
H41	0.82263	0.27268	0.76392
H42	0.18141	0.48367	0.93779
H43	0.27446	0.73216	0.89347
H44	0.77446	0.36585	0.83183
H45	0.67826	0.11797	0.84712
C46	0.45427	0.45921	0.80385
N47	0.47329	0.42259	1.03296
C48	0.4967	0.38742	0.83287
C49	0.49828	0.33915	1.0521
C50	0.43704	0.86194	0.81929
C51	0.93876	0.34324	0.67499
C52	0.51504	-0.01217	0.9927
C53	0.01594	0.50379	1.01674

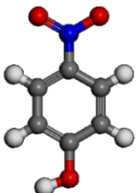
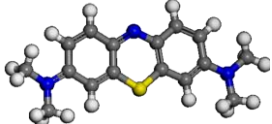
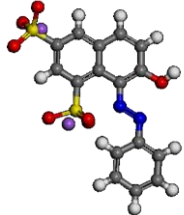
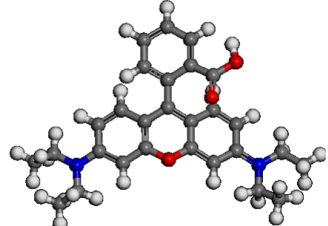
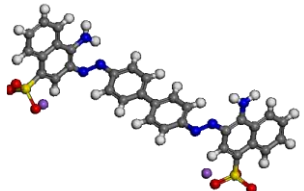
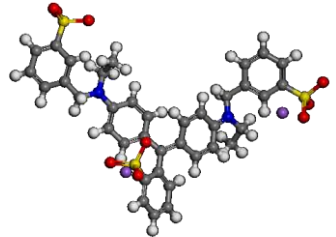
Table S3: Fractional atomic coordinates for the unit cell of TFG-TETA

Space group P1, $a = 31.58 \text{ \AA}$, $b = 33.61 \text{ \AA}$, $c = 5.99 \text{ \AA}$, $\alpha = 90.5^\circ$, $\beta = 91.2^\circ$, and $\gamma = 109.8^\circ$			
Pawley refinement $R_p = 2.16\%$, $R_{wp} = 2.62\%$			
Atom	X(\AA)	Y(\AA)	Z (\AA)
O1	0.24939	0.55466	0.54767
N2	0.32587	0.52854	0.53897
C3	0.27845	0.59752	0.46771
C4	0.32937	0.60706	0.43363
C5	0.35215	0.57375	0.48008
C6	0.35074	0.49884	0.6054
O7	0.40843	0.66014	0.31893
N8	0.35963	0.76926	0.25104
C9	0.35881	0.65094	0.35327

C10	0.33816	0.68553	0.30757
C11	0.36842	0.7282	0.21401
C12	0.33313	0.77515	0.44772
O13	0.26669	0.70963	0.29385
N14	0.17376	0.5807	0.50917
C15	0.28752	0.67627	0.34375
C16	0.2575	0.63226	0.42276
C17	0.20678	0.62406	0.45737
C18	0.12652	0.57618	0.58019
O19	0.62764	0.30317	0.25201
N20	0.54345	0.31528	0.2195
C21	0.60318	0.2568	0.29218
C22	0.55108	0.23904	0.28608
C23	0.52271	0.26773	0.23801
O24	0.4755	0.17414	0.31633
N25	0.55145	0.08352	0.46298
C26	0.52634	0.19157	0.32553
C27	0.55302	0.1618	0.37543
C28	0.52717	0.11484	0.42669
C29	0.52716	0.04096	0.56449
O30	0.63165	0.15057	0.42522
N31	0.71008	0.28908	0.30801
C32	0.60498	0.17942	0.37842
C33	0.63016	0.22672	0.3351
C34	0.68228	0.24275	0.33009
C35	0.75908	0.30178	0.24382
C36	0.37742	0.48877	0.41245
N37	0.40604	0.46342	0.49463
C38	0.42103	0.43608	0.33358
C39	0.45055	0.41054	0.41732
N40	0.46537	0.38288	0.25755
C41	0.49468	0.35827	0.34076

C42	0.51447	0.3408	0.14438
C43	0.36374	0.81248	0.59223
N44	0.38497	0.85116	0.45252
C45	0.08866	0.55095	0.41391
N46	0.04294	0.54867	0.49844
C47	0.79351	0.31276	0.44158
N48	0.84096	0.32422	0.35552
C49	0.51338	0.00464	0.38938
N50	0.49577	-0.03741	0.50588
C51	0.45171	-0.07024	0.43435
H52	0.28852	0.51733	0.53757
H53	0.18446	0.55253	0.50177
H54	0.58002	0.33128	0.25353
H55	0.41558	0.46442	0.67451
H56	0.45508	0.38097	0.07836
H57	0.04075	0.56607	0.65361
H58	0.37522	0.79631	0.13995
H59	0.36821	0.85534	0.29413
H60	0.58761	0.09235	0.42355
H61	0.69407	0.31358	0.32692
H62	0.51696	-0.04549	0.63566
C63	0.8779	0.3438	0.54906
C64	0.43147	0.88198	0.51539
C65	0.00019	0.52284	0.36731
H66	1.7697	1.12073	1.11015

Table S4: Molecular structures of the dyes used for the molecular separation experiments.

Molecule	Molecular structure	λ_{\max} nm	Charge	MW (g/mol)	Molecular size(nm)*
4-Nitrophenol		317	----	139.11	0.71 nm × 0.53 nm
Methylene blue		663	+ve	319	1.25 nm × 0.51 nm
Orange G		492	-ve	452.4	14.9 nm × 7.7 nm
Rhodamine B		552	+ve	479	1.20 nm × 1.13 nm
Congo red		504	-ve	696.7	2.56 nm × 0.53 nm
Brilliant blue		595	-ve	826	2.2 nm × 1.04 nm

* Dimension of molecules were obtained using Materials studio and some previously reported references. ^{6,7}

Table S5: Performance comparison of COF membranes with previously reported organic solvent nanofiltration membranes

Membrane	Permeance	Dye	Rejection	References
	(L m ⁻² h ⁻¹ bar ⁻¹)	(g mol ⁻¹)	(%)	
TFG-EDA	153 (Water)	Congo red (696.7)	99.2	Present work
	60 (Ethanol)	Brilliant blue (825.97)	99.5	
		Orange G (452.38)	93.4	
TFG-DETA	206 (Water)	Congo red (696.7)	99.3	Present work
	83 (Ethanol)	Brilliant blue (825.97)	99.2	
		Orange G (452.38)	92.3	
TFG-TETA	232 (Water)	Congo red (696.7)	99	Present work
	92 (Ethanol)	Brilliant blue (825.97)	99.2	
		Orange G (452.38)	90	
ZIF-8/PA	22.6 (Water)	Congo red (696.7)	99	8
S-rGO-18	103 (Water)	brilliant yellow (792.7)	86.2	9
	53 (Ethanol)	acid fuchsin (585.54)	70.1	
MPCM	30 (Water)	Rhodamine B (479)	91	7
	35 (Ethanol)	Methyl orange (327.23)	83	
		orange G (452.4)	96	
TPF-DHF (M-20)	90 (Water)	Congo red (696.7)	82	10
	60 (Ethanol)	Vitamin-12 (1,355.38)	93	
		Neutral red (288.78)	5	
Torlon & sPPSU	82.5	INCA (466)	95.5	11

		RB (1018)	99	
		AB 8(1299)	99.9	
ZnO/rGO	220 (Water)	Congo red (696.665)	98.5	¹²
		Methyl orange (327.23)	25	
		Methylene blue (319.85)	18	
Co-Ni LDHs/PEI	5.56 (Water)	Crystal violet (408)	94.4	¹³
		Methylene blue (319.85)	85	
PEIGO/PAA/PVA/GA	0.87	Congo red (696.665)	98.53	¹⁴
		Methyl blue (800)	99.5	
Polyimide (DuraMem® 150)	0.48 (Methanol)	Crystal violet (408)	97%	^{6, 15}
Polyarylate thin film (PAR-BHPF)	8 (Methanol) 8.4 (Acetone)	Crystal violet (408)	97	^{15, 16}
AOPIM-1	249.8	Rhodamine-B (479.02)	99	¹⁷
polyamide-CD (0.65)	27 (Water) 12 (Ethanol)	Methyl red (269.3)	81	¹⁸
		Brilliant blue	99	
Polybenzimidazole-M6	50 (Water) 47 (Ethanol)	Mepenzolate (420)	90	¹⁹
TFC-8	6 (Methanol)	Methyl orange (327.23)	60	²⁰
		Rose Bengal (1018)	95	
LNCM (Lysozyme)	11 (Ethanol)	orange G (452.4)	60	²¹
		acid fuschin (585.54)	98	

TpPa-Py	183(Water)	Saffranin O (350.85)	10	22
	103 (Ethanol)	Congo red (696.665)	90	
30_CO@rGO	Ethanol (40)	Brilliant blue	96	23
		Rose Bengal	90	
MPN/ZIF-8	7 (Ethanol)	Alcian blue (1298)	99	24
	22 (Methanol)	Methyl orange	55	
HI-templated (n6d)	32 (Water)	Methyl orange	98	25
	22 (Ethanol)			
HG-M1Si-T (Holey graphene)	200 (Water)	Congo red (696.65)	95.2	26
		Rhodamine-b (479)	92.4	
CMP (Conjugated microporous polymer)	12 (Ethanol)	Brilliant blue G (854)	99	27
		Rose Bengal (1,017)	99	

S14: References

1. J. H. Chong, M. Sauer, B. O. Patrick and M. J. MacLachlan, *Org. Lett.*, 2003, **5**, 3823-3826.
2. M. M. Bradford, *Anal. Biochem.*, 1976, **72**, 248-254.
3. J. Lin, C. Y. Tang, C. Huang, Y. P. Tang, W. Ye, J. Li, J. Shen, R. Van den Broeck, J. Van Impe, A. Volodin, C. Van Haesendonck, A. Sotto, P. Luis and B. Van der Bruggen, *J. Membr. Sci.*, 2016, **501**, 1-14.
4. A. M. Hung, M. Kazembeyki, C. G. Hoover and E. H. Fini, *ACS Sustainable Chem. Eng.*, 2019, **7**, 18005-18014.
5. O. M. McIntee, B. C. Welch, A. R. Greenberg, S. M. George and V. M. Bright, *Polymer*, 2022, **255**, 125167.
6. S. Karan, Z. Jiang and A. G. Livingston, *Science*, 2015, **348**, 1347-1351.
7. T. Huang, B. A. Moosa, P. Hoang, J. Liu, S. Chisca, G. Zhang, M. AlYami, N. M. Khashab and S. P. Nunes, *Nat. Commun.*, 2020, **11**, 5882.
8. L. Wang, M. Fang, J. Liu, J. He, L. Deng, J. Li and J. Lei, *RSC Adv.*, 2015, **5**, 50942-50954.
9. L. Huang, J. Chen, T. Gao, M. Zhang, Y. Li, L. Dai, L. Qu and G. Shi, *Adv. Mater.*, 2016, **28**, 8669-8674.
10. D. B. Shinde, G. Sheng, X. Li, M. Ostwal, A.-H. Emwas, K.-W. Huang and Z. Lai, *J. Am. Chem. Soc.*, 2018, **140**, 14342-14349.
11. G. Han, T.-S. Chung, M. Weber and C. Maletzko, *Environ. Sci. Technol.*, 2018, **52**, 3676-3684.
12. W. Zhang, H. Xu, F. Xie, X. Ma, B. Niu, M. Chen, H. Zhang, Y. Zhang and D. Long, *Nat. Commun.*, 2022, **13**, 471.
13. S. Zhao, H. Zhu, Z. Wang, P. Song, M. Ban and X. Song, *Chem. Eng. J.*, 2018, **353**, 460-471.
14. N. Wang, S. Ji, G. Zhang, J. Li and L. Wang, *Chem. Eng. J.*, 2012, **213**, 318-329.
15. M. F. Jimenez Solomon, Y. Bhole and A. G. Livingston, *J. Membr. Sci.*, 2012, **423-424**, 371-382.
16. T. Huang, T. Puspasari, S. P. Nunes and K.-V. Peinemann, *Adv. Funct. Mater.*, 2020, **30**, 1906797.
17. Z. Wang, X. Luo, Z. Song, K. Lu, S. Zhu, Y. Yang, Y. Zhang, W. Fang and J. Jin, *Nat. Commun.*, 2022, **13**, 4169.
18. C. Wu, H. Tan, W. Huang, W. Li, K. N. Dinh, C. Yan, W. Wei, L. Chen and Q. Yan, *Adv. Funct. Mater.*, 2020, **30**, 2003187.

19. F. Fei, L. Cseri, G. Szekely and C. F. Blanford, *ACS Appl. Mater. Interfaces*, 2018, **10**, 16140-16147.
20. Y. Li, J. Zhu, S. Li, Z. Guo and B. Van der Bruggen, *ACS Appl. Mater. Interfaces*, 2020, **12**, 31962-31974.
21. M.-B. Wu, F. Yang, J. Yang, Q. Zhong, V. Körstgen, P. Yang, P. Müller-Buschbaum and Z.-K. Xu, *Nano Lett.*, 2020, **20**, 8760-8767.
22. R. Shevate and D. L. Shaffer, *ACS Nano*, 2022, **16**, 2407-2418.
23. X. Sui, Y. Wang, F. Liu, Z. Yuan, C. Wang, Y. Yu, K. Zhou, K. Goh and Y. Chen, *Matter*, 2021, **4**, 2953-2969.
24. Y. Chen, Y. Bai, L. Meng, W. Zhang, J. Xia, Z. Xu, R. Sun, Y. Lv and T. Liu, *Chem. Eng. J.*, 2022, **437**, 135289.
25. Y. Zhang, D. Kim, R. Dong, X. Feng and C. O. Osuji, *Sci. Adv.*, 2022, **8**, eabm5899.
26. H. M. Hegab, M. Ouda, P. Kallem, C. Aubry, Y. Ibrahim, F. Banat and S. W. Hasan, *Chem. Eng. J.*, 2022, **450**, 138033.
27. B. Liang, H. Wang, X. Shi, B. Shen, X. He, Z. A. Ghazi, N. A. Khan, H. Sin, A. M. Khattak, L. Li and Z. Tang, *Nat. Chem.*, 2018, **10**, 961-967.